



AFRL-OSR-VA-TR-2013-0535

RESEARCH STUDIES ON PHOTONS AND BIPHOTONS

STEPHEN HARRIS

LELAND STANFORD JUNIOR UNIVERSITY

**10/01/2013
Final Report**

DISTRIBUTION A: Distribution approved for public release.

**AIR FORCE RESEARCH LABORATORY
AF OFFICE OF SCIENTIFIC RESEARCH (AFOSR)/RSE
ARLINGTON, VIRGINIA 22203
AIR FORCE MATERIEL COMMAND**

REPORT DOCUMENTATION PAGE

Form Approved
OMB No. 0704-0188

Public reporting burden for this collection of information is estimated to average 1 hour per response, including the time for reviewing instructions, searching existing data sources, gathering and maintaining the data needed, and completing and reviewing this collection of information. Send comments regarding this burden estimate or any other aspect of this collection of information, including suggestions for reducing this burden to Department of Defense, Washington Headquarters Services, Directorate for Information Operations and Reports (0704-0188), 1215 Jefferson Davis Highway, Suite 1204, Arlington, VA 22202-4302. Respondents should be aware that notwithstanding any other provision of law, no person shall be subject to any penalty for failing to comply with a collection of information if it does not display a currently valid OMB control number. **PLEASE DO NOT RETURN YOUR FORM TO THE ABOVE ADDRESS.**

1. REPORT DATE (DD-MM-YYYY) 01-10-2013		2. REPORT TYPE Final	3. DATES COVERED (From - To) 03/15/2010-09/14/2013		
4. TITLE AND SUBTITLE RESEARCH STUDIES ON PHOTONS AND BIPHOTONS			5a. CONTRACT NUMBER FA9550-10-1-0055		
			5b. GRANT NUMBER		
			5c. PROGRAM ELEMENT NUMBER		
6. AUTHOR(S) Professor Stephen Harris			5d. PROJECT NUMBER		
			5e. TASK NUMBER		
			5f. WORK UNIT NUMBER		
7. PERFORMING ORGANIZATION NAME(S) AND ADDRESS(ES) Stanford University			8. PERFORMING ORGANIZATION REPORT NUMBER 009214214		
9. SPONSORING / MONITORING AGENCY NAME(S) AND ADDRESS(ES) Air Force Office of Scientific Research			10. SPONSOR/MONITOR'S ACRONYM(S)		
			11. SPONSOR/MONITOR'S REPORT NUMBER(S)		
12. DISTRIBUTION / AVAILABILITY STATEMENT approved for public release					
13. SUPPLEMENTARY NOTES					
14. ABSTRACT The central theme of the work on this contract has been: development of techniques and ideas for the control of the waveforms of single photons and the extension of the concepts of nonlinear optics into the x-ray portion of the electromagnetic spectrum. Advances in the first portion of this work include: the first demonstration of use of spread spectrum technology at the single photon level, and in particular the demonstration that it is possible to hide a single photon in an environment of a much higher density of photons with the same spectral power density, and the first demonstration of the technique of chirp and compress, again at the level of a single photon. Key contributions and advances in the hard x-ray portion of this work include: The invention of a new technique for the generation of polarization entangled x-ray biphotons (theoretical), and the demonstration of parametric down conversion in the Langevin regime. Recently, a paper describing the first demonstration of second harmonic generation at x-ray wavelengths has been submitted.					
15. SUBJECT TERMS single photons; spread spectrum; nonlocal dispersion; nonlinear x-ray processes; x-ray second harmonic and mixing					
16. SECURITY CLASSIFICATION OF:			17. LIMITATION OF ABSTRACT 49	18. NUMBER OF PAGES	19a. NAME OF RESPONSIBLE PERSON Professor Stephen Harris
a. REPORT U	b. ABSTRACT U	c. THIS PAGE U			19b. TELEPHONE NUMBER (include area code) 650-725-2248

Final Performance Report

RESEARCH STUDIES ON PHOTONS AND BIPHOTONS

Grant AFOSR FA9550-10-1-0055

Prepared for

**AIR FORCE OFFICE OF SCIENTIFIC RESEARCH
and
ARMY RESEARCH OFFICE**

For the Period

March 15, 2010 to September 14 2013

Submitted by

S. E. Harris¹, Principal Investigator

**Edward L.Ginzton Laboratory
Stanford University**

¹seharris@stanford.edu

Contents

1	Executive Summary	3
2	Publications and Presentations	4
2.1	Publications	4
2.2	Presentations	5
2.3	Patent Disclosure	6
3	Abstracts of Published Papers	7
3.1	Hiding Single Photons with Spread Spectrum Technology	7
3.2	Generation and Compression of Chirped Biphotons	7
3.3	Polarization Entangled Photons at X-Ray Energies	7
3.4	Ultrabright Backward Wave Biphoton Source	7
3.5	A miniature ultrabright source of temporally long, narrowband biphotons . .	8
3.6	X-Ray Parametric Down-Conversion in the Langevin Regime	8
3.7	X-ray and optical wave mixing	8
4	X-Ray Second Harmonic Generation	9
4.1	Introduction	9
4.2	Experiment	12
4.3	Results	13
5	Temporal and Spatial Correlation of x-ray biphotons	17
5.1	Coupled Operator Equations	18
5.2	Solution	20
5.3	Signal and idler count rates	21
5.4	Correlations and coincidence counts	22
5.5	Δk_z in the Laue geometry	23

6	Appendix: Cavity-Enhanced SPDC	23
6.1	Nonlinear Polarizations	24
6.2	SVEA (Lamb) Equations	27
6.3	Standing Wave	29
6.4	Traveling Wave	29
6.5	Quantized coupled SVEA (Lamb) Equations	30
6.6	Power Conservation	31
6.7	With Pump	32
6.8	Output Fields	33
6.9	Spatial Coupling Factor and Gaussian Beam	37
6.10	Paired Count Rate and Spectral Power Density	39
6.11	Temporal Second-order Intensity Correlation Function	41
6.12	SPDC with Quasi-Phase Matched Backward-wave	42
6.13	Practical Considerations	46
6.14	Single Longitudinal-mode	46
6.15	Tuning Rate	46
6.16	Mode Hoping	47
6.17	Stabilization	47
6.18	Coherence Length and Bandwidth	47
6.19	Paired Count Rate and Spectral Brightness	48
6.20	Without Cavity	48

1 Executive Summary

The central theme of the work on this contract has been: 1) the development of techniques and ideas for the control of the waveforms of single photons and, 2) the extension of the concepts of nonlinear optics into the x-ray portion of the electromagnetic spectrum. Advances in the first portion of this work include: the first demonstration of use of spread spectrum technology at the single photon level (Belthangady et al.); and in particular the demonstration that it is possible to hide a single photon in an environment of a much higher density of photons with the same spectral power density, and 2) The first demonstration of the technique of chirp and compress, again at the level of a single photon (Sensarn et al.). Key contributions and advances in the hard x-ray portion of this work include: 1) The invention of a new technique for the generation of polarization entangled x-ray biphotons (Shwartz et al.). 2) The demonstration of parametric down conversion in the Langevin regime. 3) The first demonstration of x-ray optical mixing. (This work was part of a team led by Ernie Glover. 4) And very recently, the first demonstration of second harmonic generation at x-ray wavelengths. Additional contributions include the demonstration of a greatly simplified technique for obtaining temporally long biphotons (Chih-Sung Chuu), as well as the suggestion of a second, backward wave technique that has not yet been demonstrated.

In the following sections we follow the AFOSR final report guideline and will not repeat already published and well documented work. For completeness, in these cases, we will include the published abstract. When the work is still underway, and not published or not completely published, we expand and give details here.

We note that this work has been jointly supported by the US Army Research Office. Before this contract began, we were jointly supported by DARPA, and the work described here benefited from that interaction.

We begin by summarizing Publications and Presentations during this contract period.

2 Publications and Presentations

2.1 Publications

- (1) Chinmay Belthangady, Chih-Sung Chuu, Ite A. Yu, G.Y. Yin, J. M. Kahn, and S. E. Harris, “Hiding Single Photons with Spread Spectrum Technology,” *Phys. Rev. Lett.*, **104**, 223601, (June 4, 2010).
- (2) S. Sensarn, G. Y. Yin, and S. E. Harris, “Generation and Compression of Chirped Biphotons,” *Phys. Rev. Lett.*, **104**, 253602, (June 25, 2010).
- (3) S. Shwartz and S.E. Harris, “Polarization Entangled Photons at X-Ray Energies,” *Phys. Rev. Lett.* **106**, 080501, 2011.
- (4) Chih-Sung Chuu and S.E. Harris, “ Ultrabright Backward Wave Biphoton Source”, *Phys. Rev. A*, **83**, 061803R, 2011.
- (5) S. Shwartz, R.N. Coffee, J.M. Feldkamp, Y. Feng, J.B. Hastings, G.Y. Yin, and S.E. Harris, “X-Ray Parametric Down-Conversion in the Langevin Regime”, *Phys. Rev. Lett.*, **109**, 013602, (July 6, 2012).
- (6) Chih-Sung Chuu, G. Y. Yin, and S. E. Harris, “A miniature ultrabright source of temporally long, narrowband biphotons,” *Appl. Phys. Lett.*, **101**, Q51108 (2012).
- (7) T. E. Glover, D. M. Fritz, M. Cammarata, T. K. Allison, Sinisa Coh, J. M. Feldkamp, H. Lemke, D. Zhu, Y. Feng, R. N. Coffee, M. Fuchs, S. Ghimire, J. Chen, S. Shwartz, D. A. Reis, S. E. Harris & J. B. Hastings, “X-ray and optical wave mixing, *Nature*, **488**, 603, (29 August 2012).
- (8) S. Shwartz, M. Fuchs, J. B. Hastings, Y. Inubushi, T. Ishikawa, T. Katayama, D. A. Reis, T. Sato, K. Tono, M. Yabashi, and S. E. Harris, “X-Ray Second Harmonic Generation ”, (submitted for publication).
- (9) Steven Sensarn “Nonlocal Modulation and Dispersion ”, PhD dissertation, (May 2010).
- (10) Chinmay Belthangady “Amplitude and Phase Modulation of Single Photons and Biphotons”, PhD dissertation, (June 2010).

The paper “Polarization Entangled Photons at X-Ray Energies” was upgraded by the reviewers from a PRA to Physical Review Letters, and the paper “Ultrabright Backward

Wave Biphoton Source” was selected by the editors for a Physics Viewpoint (spotlighting exceptional research).

2.2 Presentations

- (1) S. Shwartz and S. E. Harris, “Generation of Polarization Entangled Photons at X-Ray Energies”, SPRC 2010 Annual Symposium, Stanford, CA (September 13, 2010) (invited).
- (2) S. E. Harris, “Modulation of Photons and Biphotons, Texas A&M, November 2010.
- (3) Chih-Sung Chuu, Chinmay Belthangady, Ite A. Y, G.Y. Yin, J. M. Kahn, and S.E. Harris, ”Spread Spectrum Technology with Single Photons and Slow Light, SPIE Photonics West, San Francisco, CA (January 22-27, 2011) [invited].
- (4) Chih-Sung Chuu, Chinmay Belthangady, Ite A. Y, G.Y. Yin, J. M. Kahn, and S.E. Harris, Hiding Single Photons with Spread Spectrum Technology, 42nd Annual Meeting of the Division of Atomic, Molecular, and Optical Physics (APS-DAMOP-2011), Atlanta, GA (June 13, 2011).
- (5) S. Shwartz and S. E. Harris, ”Polarization Entangled Photons at X-Ray Energies”, OSA Topical Meeting on Nonlinear Optics (NLO), Kauai, HI (July 17, 2011).
- (6) Chih-Sung Chuu and Steve Harris, ”Ultra-bright Backward Wave Biphoton Source”, OSA Topical Meeting on Nonlinear Optics (NLO), Kauai, HI (July 17, 2011).
- (7) S.E. Harris, Modulation of Photons and Biphotons, OSA Topical Meeting on Nonlinear Optics (NLO), Kauai, HI (July 17, 2011) [plenary].
- (8) S. Shwartz, ”X-ray Nonlinear Optics in Crystals”, LCLS/SSRL users’ meeting SLAC, CA (2011) (Invited).
- (9) S. Shwartz, R. N. Coffee, J. M. Feldkamp, Y. Feng, J. B. Hastings, G. Y. Yin, and S. E. Harris, ”X-Ray Parametric Down-Conversion in The Langevin Regime”, Winter Colloquium on the Physics of Quantum Electronics (PQE), Snowbird, Utah (January 2012) (Invited).

- (10) Chih-Sung Chuu,,Generation and Modulation of Temporally Long Single Photons and Biphotons, Physics colloquium, Physics Department, National Tsing Hua University, Hsinchu, Taiwan, February 22, 2012.
- (11) Chih-Sung Chuu,, Manipulating the wavepackets of single photons and biphotons, Physics colloquium, Physics Department, National Chung Cheng University, Chiayi, Taiwan, March 21, 2012.
- (12) S. Shwartz and S. E. Harris, ” Parametric Down-Conversion at X-Ray Wavelengths”, International Workshop on Atomic Physics 2012, Dresden, Germany (November 2012) (Invited).
- (13) Chih-Sung Chuu,, Shaping single photons and biphotons, Colloquium, Electrophysics Department, National Chia Tung University, Hsinchu, Taiwan, November 15, 2012.
- (14) Chih-Sung Chuu,,Shaping single photons and biphotons, Colloquium, Physics Department, National Taiwan Normal University, Taipei, Taiwan, December 19, 2012.
- (15) Chih-Sung Chuu Shaping single photons and biphotons, Colloquium, Physics Department, National Cheng Kung University, Tainan, Taiwan, January 4, 2013.
- (16) Chih-Sung Chuu, Shaping single photons and biphotons, Colloquium, Institute of Physics, National Chia Tung University, Hsinchu, Taiwan, January 3, 2013.
- (17) S. Shwartz, M. Fuchs, J. B. Hastings, Yuichi Inubushi, T. Ishikawa, T. Katayama, D. A. Reis, T. Sato, K. Tono, M. Yabashi, and S. E. Harris, Second Harmonic Generation at X-Ray Wavelengths, OSA Topical Meeting on Nonlinear Optics, Kona, HI (July 2013). (Invited)
- (18) S.E. Harris “Fifty Years of Parametric Down Conversion: From Microwaves to x-rays, CLEO-QELS, San Jose , CA, (June 2013 [plenary]).

2.3 Patent Disclosure

“Ultrabright long biphoton generation with non-linear optical material” , S11-432/US–PID:18566

3 Abstracts of Published Papers

3.1 Hiding Single Photons with Spread Spectrum Technology

Authors: Chinmay Belthangady, Chih-Sung Chuu, Ite A. Yu, G.Y. Yin, J.M. Kahn, and S.E. Harris

We describe a proof-of-principal experiment demonstrating the use of spread spectrum technology at the single photon level. We show how single photons with a prescribed temporal shape, in the presence of interfering noise, may be hidden and recovered.

3.2 Generation and Compression of Chirped Biphotons

Authors: S. Sensarn, G. Y. Yin, and S. E. Harris

We describe an experiment demonstrating the radarlike technique of chirp and compress. Chirped biphotons are generated using a quasi-phase-matched nonlinear crystal where the phase-matched frequency varies linearly with position. Sum frequency generation is used to measure the amplitude of the biphoton wave function. As compared to a nonchirped crystal, compression and an increase in summing efficiency of a factor of 5 is observed.

3.3 Polarization Entangled Photons at X-Ray Energies

Authors: S. Shwartz and S.E. Harris

We show that polarization entangled photons at x-ray energies can be generated via spontaneous parametric down-conversion. Each of the four Bell states can be generated by choosing the angle of incidence and polarization of the pumping beam.

3.4 Ultrabright Backward Wave Biphoton Source

Authors: Chih-Sung Chuu and S.E. Harris

We calculate the properties of a biphoton source based on resonant backward-wave spontaneous parametric down conversion. We show that the biphotons are generated in a single longitudinal mode having a subnatural linewidth and a Glauber correlation time exceeding 65 ns.

3.5 A miniature ultrabright source of temporally long, narrow-band biphotons

Authors: Chih-Sung Chuu, G. Y. Yin, and S. E. Harris,

We demonstrate a miniature source of long biphotons utilizing the cluster effect and double-pass pumping in a monolithic doubly resonant parametric down-converter. We obtain a biphoton correlation time of 17.1ns with a generation rate of 1.1×10^5 biphotons/(s mW) and an estimated linewidth of 8.3 MHz.

3.6 X-Ray Parametric Down-Conversion in the Langevin Regime

Authors: S. Shwartz, R.N. Coffee, J.M. Feldkamp, Y. Feng, J.B. Hastings, G.Y. Yin, and S.E. Harris

We experimentally and theoretically study the coincidence count rate for down-converted x-ray photons. Because of photoionization, parametric down-conversion at x-ray wavelengths generally involves loss and the theoretical description requires a Langevin approach. By working in a transmission geometry (Laue) rather than in the Bragg geometry of previous experiments, we obtain an improvement in the signal-to-noise ratio of 12.5, and find agreement between experiment and theory.

3.7 X-ray and optical wave mixing

Authors: T. E. Glover, D. M. Fritz, M. Cammarata, T. K. Allis, Sinisa Coh, J. M. Feldkamp, H. Lemke, D.Zhu, Y. Feng, R. N. Coffee, M. Fuchs, S. Ghimire, J. Chen, S. Shwartz, D. A. Reis , S.E.Harris, and J. B. Hastings

Lightmatter interactions are ubiquitous, and underpin a wide range of basic research fields and applied technologies. Although optical interactions have been intensively studied, their microscopic details are often poorly understood and have so far not been directly measurable. X-ray and optical wave mixing was proposed nearly half a century ago as an atomic-scale probe of optical interactions but has not yet been observed owing to a lack of sufficiently intense X-ray sources. Here we use an X-ray laser to demonstrate X-ray and optical sum-frequency generation. The underlying nonlinearity is a reciprocal-space probe of the optically

induced charges and associated microscopic fields that arise in an illuminated material. To within the experimental errors, the measured efficiency is consistent with first-principles calculations of microscopic optical polarization in diamond. The ability to probe optical interactions on the atomic scale offers new opportunities in both basic and applied areas of science

4 X-Ray Second Harmonic Generation

Our work on second harmonic generation has now been submitted for publication . The authors of the submitted publication are: S. Schwartz, M. Fuchs, J. B. Hastings, Y. Inubushi, T. Ishikawa, T. Katayama, D. A. Reis, T. Sato, K. Tono, M. Yabashi, S. Yudovich, and S. E. Harris. An excerpt and summary of this paper follows:

4.1 Introduction

This work reports experimental evidence for coherent nonlinear x-ray interaction at intensities on order of 10^{16} W/cm², where the corresponding electric field approaches the atomic-field strength. Using a 1.7 Angstrom pump beam we observed second harmonic generation in diamond without permanent damage. The generated second harmonic is of order ten times the background radiation, scales quadratically with pump pulse-energy, and is generated over a narrow phase-matching condition. Our observation of a nonlinear effect at intensities that are several orders of magnitude higher than the radiation damage threshold in the visible regime forms a basis for more general nonlinear experiments in the area of x-ray nonlinear optics.

It is now 40 years since Freund and Eisenberger and colleagues described a theory for the nature of a solid-state dense plasma nonlinearity that is operative at x-ray wavelengths. This nonlinearity is nonlocal and of the second order and may be observed in centro-symmetric materials but requires a nonuniform electron density. Because of the small magnitude of this nonlinearity, to date, all experiments have been based on parametric down conversion from the vacuum. The key factor for those experiments is the large number of vacuum fluctuation modes at x-ray wavelengths. Thus, although the parametric gain is very small, coincidences

of the generated signal and idler photons can be measured even when the pump source is an x-ray tube. Recently, Glover and colleagues have demonstrated the nonlinear wave mixing of x-ray and near-infrared beams using an x-ray FEL. However, the efficiency in this depends on the intensity of the infrared laser and not on the intensity of the x-ray laser. On the other hand, the high peak power an x-ray FEL is critical for the observation of most x-ray coherent nonlinear effects.

Here we report the phase-matched second harmonic generation at hard x-ray wavelengths. Using a 1.7 Å (7.3 keV) pump beam from the SACLA FEL at an intensity of 10^{16} W/cm² the observed second harmonic is generated in a crystal of diamond. The observed second harmonic (SH) signal is about 1 photon every 150 x-ray laser shots each containing about a billion 7.3 keV photons focused to a micron-sized spot on the crystal. The second harmonic beam is generated in a narrow angular range of 0.2 mrad full-width at half maximum (FWHM) and scales quadratically with pump-pulse energy.

The weakness of the process, even with focused x-ray fields on the order of the atomic-field strength, requires careful attention to reduce or eliminate potential backgrounds. In particular, we designed the experiment to suppress the off-axis second harmonic in the pump beam generated in the free-electron laser process itself as well as well parasitic scatter of the fundamental pump. At hard x-ray wavelengths, phase matching can be achieved by using the periodic nature of the electron density in crystals. Phase matching occurs when $2\vec{k}_\omega + \vec{G} = k_{2\omega}$ where \vec{k}_ω and $k_{2\omega}$ are the internal wavevectors of the pump and second harmonic beams respectively and \vec{G} is a reciprocal lattice vector. Because of the finite dispersion, the angles between the beams and the atomic planes differ slightly from the linear Bragg diffraction condition of the second harmonic. However, the expected offsets are small compared to both the divergence of the focused pump beam and the measured width of the SH signal. This presents a challenge for distinguishing SHG from the linear Bragg diffraction of the residual SH in the pumping beam.

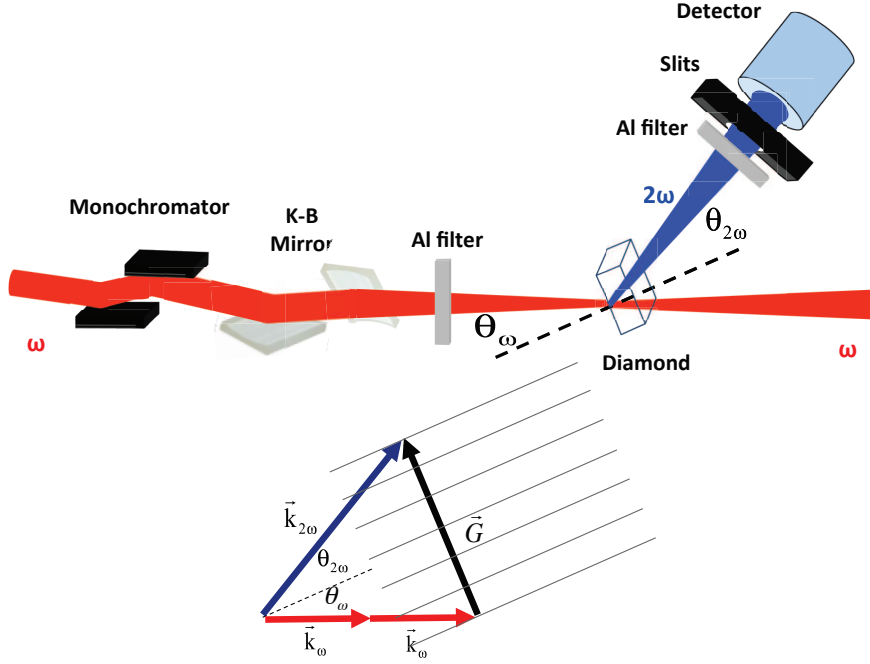


Figure 1: Schematic of the SHG experimental setup. X-ray pulses from the SACLA free electron laser are incident a silicon (111) channel cut monochromator at 10Hz. The monochromator selects a 7.3 keV pump-beam with 1eV bandwidth while rejecting a substantial fraction of the second harmonics. A pair of Kirkpatrick Baez mirrors focuses the beam to about 1.5 microns while reducing the third harmonic contamination. The nonlinear medium is a (111) cut diamond crystal placed in the focus and set for phase matching as indicated in the phase matching diagram (bottom). The phase matching is achieved by using the (220) atomic planes; k_{ω} and $k_{2\omega}$ are the wave vectors of the pump and the generated second harmonic respectively. G is the reciprocal lattice vector orthogonal to the (220) atomic planes. We control the intensity of the pump by using a set of Al filters before the sample.

4.2 Experiment

The experiment was performed at BL3 SPring-8 Angstrom Compact free electron laser (SACLA) in Hyogo, Japan. The experimental setup is shown schematically in Fig 1.

In order to observe the SHG generated in the crystal extreme care was required to suppress backgrounds from residual second harmonic contribution in the beam and parasitic scattering of the fundamental into the detector as well as orient the sample and detector. A Si (111) double-crystal monochromator is used to select a narrow (1eV) bandwidth pump-beam centered at 7.3 keV photon energy from the FEL. While even harmonics are forbidden by symmetry from being radiated on axis, there is a finite SH generated slightly off-axis due to the highly relativistic motion of the electrons in the undulator. The monochromator suppresses the second harmonic by more than four orders of magnitude because the second order Si (222) Bragg peak is very nearly forbidden. After monochromatization the beam is focused by a pair of grazing incidence mirrors in the Kirkpatrick-Baez (KB) geometry to about 1.5 m FWHM spot at the sample (assuming a Gaussian beam, the Rayleigh range is 30 mm and the divergence is 41 rad). A set of thin Al filters before the KB mirrors are used to attenuate the fundamental while having negligible effect on the residual harmonic. The pulse energy after the filters is measured on a shot-by-shot basis. The sample is a 0.48 mm thick (111) cut diamond single crystal and is placed in the focus of the x-ray beam. The sample is oriented near the diffraction condition for the (220) planes in the symmetric Laue geometry with the polarization of the pump in the scattering plane. In this geometry both diffracted residual second harmonic and the generated second harmonic transmit through the crystal. Scattered photons are detected by a YAP:Ce scintillation detector with energy resolution of 30. We choose to phase-match with the (220) reciprocal lattice vector. Importantly, this corresponds to the (110) planes for the fundamental which is strictly forbidden in the face-center cubic structure, and thus elastic scattering of the pump in the direction of the second harmonic generation is very highly suppressed. Nonetheless, as we expect average count rates of much less than a single second harmonic photon per FEL pulse, additional suppression is necessary. Note that the detector cannot distinguish a single SH photon from two fundamental photons on any given pulse. Moreover, the probability of measuring two

photons per pulse also scales quadratically with incident pulse energy (as is the expected SHG signal), so the suppression of stray scattered fundamental photons is critical. We use slits and a set of Al foils between the sample and the detector to restrict the solid angle of the detector and filter out background photons at the fundamental wavelength. The Al filters attenuate the background at the fundamental wavelength by a factor of 10^6 , while the SHG beam is attenuated by a factor of 6.75.

4.3 Results

Since the maximum intensity in our experiment was about 10^{16} W/cm², we first checked for damage by measuring the elastic scattering of the (220) peak at 7.3 KeV at the maximum pulse energy and observed no changes in the peak reflectivity or in the rocking curve. We conclude that the crystal structure did not change during the exposure to the XFEL beam.

A histogram of detector counts as a function of photon energy is shown in Fig. 2a at full intensity (no filter before the diamond crystal) and at the peak of the phase matching condition for 24000 shots. The energy bin width is 1.39 keV. The data of Fig 2a consists primarily of two peaks corresponding to photon energies near the fundamental and SH. There is a small possibility of detected third harmonic photons as well. If we apply upper and lower-level thresholds for defining a SH photon as 10.2^{-19} KeV (+/- 30% of 14.6 keV), we measure 153 SH photons in 24000 pulses (0.00640.0005/pulse), compared to 35 fundamental photons in 5.19.5 keV (0.00150.0002/pulse). This level is low enough that contamination from the wings of the fundamental (or third harmonic) is small, and the probability of two fundamental photons in a single pulse is negligible.

In order to determine whether the second harmonic photons are generated in the crystal or due to elastic scattering, We insert a 0.0025 mm Al filter before the diamond crystal in order to determine whether the SH photons are generated in the crystal or due to elastic scattering from the residual harmonic content in the incident beam. The absorption coefficients for Al at the fundamental and SH are 168.0 cm⁻¹ and 21.8 cm⁻¹ corresponding to transmission through the pre-filter of 0.43 and 0.9 respectively. The resulting histogram is plotted in Fig. 2b. In this case we count only 7 second harmonic photons in 6000 pulses, 207 % of what

one would expect if the signal was solely from undulator SH. This indicates that most of the signal at the highest pump pulse-energy is SH generated in the crystal. In fact, if the SH signal scales quadratically with pulse energy, than the signal upon inserting the Al filter should be reduced by a factor of slightly more than five to 18.5%.

To better quantify the background we repeat the measurement with 0.025 mm, 0.1 mm, and 0.2 mm thick Al filters and with no filter. Fig. 3a shows the SH count rate as a function of the average of the pump pulse-energy when the crystal is detuned by -57 rad from the peak of the phase matching condition. Fig 3b shows the rocking curve of the SHG process, namely, the SH count rate as a function of the angular deviation of the crystal from the phase matching angle taken without filters. Consistent with the data on the peak of the phase matching condition, the SH signal at -57 rad (Fig 3a) upon inserting the 0.025 mm pre-filter is reduced to 18.8 % of the value without the filter. It is clear from Fig. 3a that the count rates at the two lowest pulse energies are equal within the statistical error. We use this to estimate the residual SH assuming that it dominates the measurement at the lowest pulse-energy. After correcting for the filter transmission, we find that the residual harmonic corresponds to 0.00540.0030 counts/pulse. Thus the SHG from the crystal is about a factor of ten higher than the background at the highest intensity. Assuming that the background is negligible at all angles, the width of the curve represents the width over which the second harmonic is phase matched. We plot a Gaussian fit and find the FWHM of the rocking curve is about 180 μ rad.

In summary, we report experimental evidence for phase matched SHG at hard x-ray wavelengths. The magnitude of the generated SH energy scales as the square of the pump pulse energy, and its magnitude peaks at the calculated phase matching angle. The largest observed SHG efficiency is 5.8×10^{-11} , with an observed count rate that is more than ten times above the background noise. These results advance our understanding of coherent x-ray matter interactions at high intensity and form the basis for more general experiments on x-ray nonlinear processes. For example, future experiments might explore x-ray phase conjugation, squeezing, and the generation of polarization entangled x-ray photons.

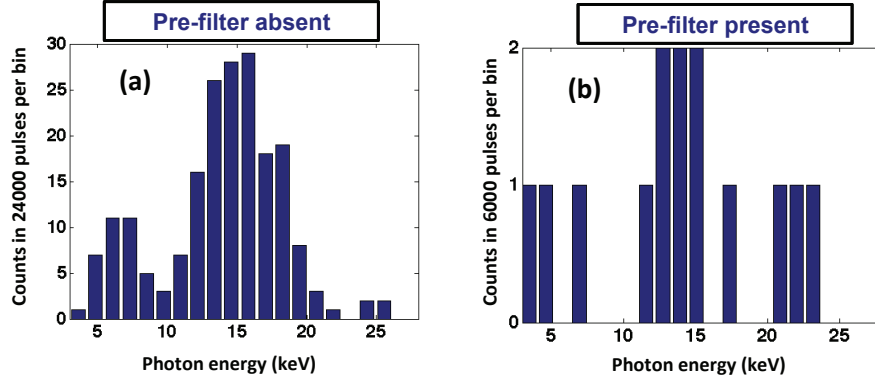


Figure 2: Photon-energy histograms of the measured signal at the peak of the phase-matching condition. The pump-photon-energy is 7.3 keV and the SHG photon-energy is 14.6 keV. The energy resolution of the detector is 30 %. The data in part (a) are taken with no attenuation. The data in part (b) are taken with a 0.025 mm Al filter before the diamond crystal (the transmission through the filter is 0.43 and 0.9 at 7.3 keV and at 14.6 keV respectively). In Fig. 2b the second harmonic count rate is 20 percent of what would be expected if it resulted from the undulator alone. Note that the number counts per pulse is small, and the second harmonic counts are larger than the counts at the fundamental frequency; thus, the contribution from two simultaneous fundamental photons is negligible.

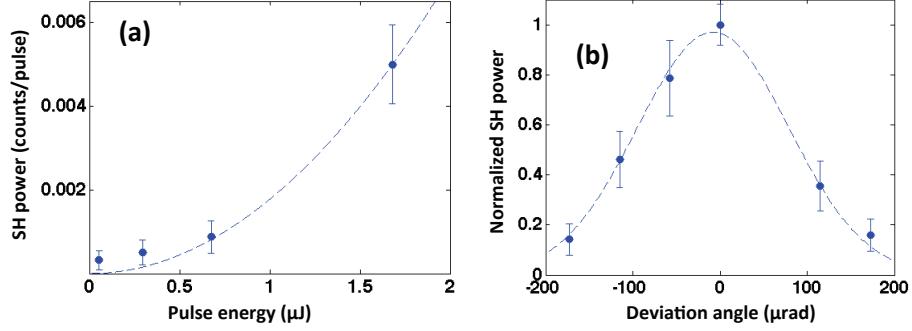


Figure 3: Scaling of second harmonic rate with average pump pulse-energy and deviation angle. (a) Detected second harmonic signal as a function of input pulse-energy and measured at angular deviation of $-57 \mu\text{ rad}$ from the SHG phase-matching angle. The pulse-energy is varied by inserting thin Al filters in the beam before the diamond crystal. Each of the measured data points represents an average over 6000 pulses. The dashed blue curve is calculated from the theory and scaled vertically by a factor of 1.48. The second harmonic contribution at the higher pulse energies (two points) is dominated by SHG, while at the lower pulse energies the residual second harmonic contamination dominates. (b) Normalized second harmonic signal as a function of the angular deviation of the diamond crystal from the phase matching angle. The data in part (b) are obtained with no attenuation before the diamond crystal. The dashed curve is a Gaussian fit to the experimental data. The FWHM of the rocking curve is $180 \mu\text{ rad}$. The peak point represents the average signal measured over 2400 pulses. The other points represent the average signal measured over 6000 pulses. In both plots, the vertical error bars indicate the counting statistics.

5 Temporal and Spatial Correlation of x-ray biphotons

It is the intent of this Section to derive and summarize the formulae for the temporal and spatial correlations that are inherent to the spontaneous downconversion of an incident near-monochromatic x-ray pumping beam. When combined with further numerical work, it is likely, but not certain that we will submit the work of this section for publication. This section was written by S.E. Harris.

We begin by developing the coupled equations for this inherently non-collinear problem. To start, we separate the driving term of the wave equation into a polarization \mathcal{P} that is linear in the driving e-field and a driving current density \mathcal{J} that is quadratic in the driving e-fields. With $\vec{\nabla}_\perp = \vec{a}_x \frac{\partial}{\partial x} + \vec{a}_y \frac{\partial}{\partial y}$, the wave equation in free space is

$$\frac{\partial^2 \mathcal{E}}{\partial z^2} + \nabla_\perp^2 \mathcal{E} - \frac{1}{c^2} \frac{\partial^2 \mathcal{E}}{\partial t^2} = \mu_0 \frac{\partial^2 \mathcal{P}}{\partial t^2} + \mu_0 \frac{\partial \mathcal{J}}{\partial t}. \quad (5.1)$$

With $\mathbf{r} = \{x, y\}$, and $\mathbf{q} = \{k_x, k_y\}$, we Fourier Transform Eq. (1) so that $\mathcal{E}(z, x, y, t) \rightarrow \tilde{E}(z, k_x, k_y, \omega)$, $\mathcal{P}(z, x, y, t) \rightarrow \tilde{P}(z, k_x, k_y, \omega)$ and $\mathcal{J}(z, x, y, t) \rightarrow \tilde{J}(z, k_x, k_y, \omega)$. For example,

$$\mathcal{E}(z, \mathbf{r}, t) = \int_{-\infty}^{\infty} \int_{-\infty}^{\infty} \tilde{E}(z, \mathbf{q}, \omega) \exp[-i(\omega t - \mathbf{q} \cdot \mathbf{r})] \mathbf{d}\mathbf{q} d\omega \quad (5.2)$$

We substitute Eq.(2) into Eq.(1) and write the linear portion of the frequency domain dipole moment in terms of the refractive index $\tilde{P}(\omega) = \epsilon_0[n(\omega)^2 - 1]\tilde{E}(\omega)$. With $k^2(\omega) \equiv \omega^2 n^2(\omega)/c^2$, the Fourier transform of Eq.(1) is

$$\frac{\partial^2 \tilde{E}}{\partial z^2} - (k_x^2 + k_y^2) \tilde{E} + k^2(\omega) \tilde{E} = -i\mu_0 \omega \tilde{J}. \quad (5.3)$$

Eq.(3) is exact and contains dispersion to all orders.

It is often the case that the electromagnetic fields vary slowly in the z-direction as compared to the x-ray wavelength. It is then useful to the change variable from

$$\begin{aligned} \tilde{E} &= E(z) \exp(ik_z z) \\ \tilde{J} &= J(z) \exp(ik_z z) \end{aligned} \quad (5.4)$$

With $k_x^2 + k_y^2 + k_z^2 = k^2(\omega) = \omega^2 n(\omega)^2/c^2$, and assuming that $\partial^2 E/\partial z^2 \ll k_z \partial E/\partial z$ we obtain the equation for the slowly varying Fourier components of the electromagnetic fields.

With the impedance $\eta(\omega) = \sqrt{(\mu_0/\epsilon_0)n(\omega)}$, and an angle of propagation θ_z with regard to the z axis, we have

$$\cos(\theta_z)\partial E/\partial z = -\frac{\eta}{2}J \quad (5.5)$$

In the following we will assume that the signal and idler fields are described by the prototype plasma nonlinearity as first described by Levine and Eisenberger []. This nonlinearity is dependent on whether the various fields are polarized in, or out, of the plane of incidence [], and generally leads to the generation of polarization entangled photons []. This nonlinearity satisfies detailed balance, so that with $\zeta(\omega_s, \omega_i, \omega_p) \equiv \zeta$, $\tilde{J}_s = \omega_s \zeta \tilde{E}_p \tilde{E}_i^*$, $\tilde{J}_i = \omega_i \zeta \tilde{E}_p \tilde{E}_s^*$, and $\tilde{J}_p = -\omega_p \zeta \tilde{E}_s \tilde{E}_i$. Following the transformation of Eq.(4), the nonlinearity as it appears in the first of the coupled S.V.E.A. equations is $J_s = \omega_s \zeta E_p E_i^* \exp(i\Delta k_z z)$ where

$$\Delta k_z = k_{pz} - (k_{sz} + k_{iz}) \quad (5.6)$$

The coupled S.V.E.A. equations for the signal, idler, and pump fields are

$$\begin{aligned} \cos(\theta_s)\frac{\partial E_s}{\partial z} + \alpha_s E_s &= -\frac{\omega_s \eta_s \zeta}{2} E_p E_i^* \exp(i\Delta k_z z) \\ \cos(\theta_i)\frac{\partial E_i}{\partial z} + \alpha_i E_i &= -\frac{\omega_i \eta_i \zeta}{2} E_p E_s^* \exp(i\Delta k_z z) \\ \cos(\theta_p)\frac{\partial E_p}{\partial z} + \alpha_p E_p &= \frac{\omega_p \eta_p \zeta}{2} E_s E_i \exp(-i\Delta k_z z) \end{aligned} \quad (5.7)$$

With the loss at all frequencies taken as zero, and with θ as the angle with the z-axis these equations satisfy the photon conservation condition

$$\begin{aligned} \cos(\theta_s) \left[\frac{1}{\omega_s} \frac{d}{dz} \left(\frac{|E_s|^2}{2\eta_s} \right) \right] &= \cos(\theta_i) \left[\frac{1}{\omega_i} \frac{d}{dz} \left(\frac{|E_i|^2}{2\eta_i} \right) \right] = \\ - \cos(\theta_p) \left[\frac{1}{\omega_p} \frac{d}{dz} \left(\frac{|E_p|^2}{2\eta_p} \right) \right] \end{aligned} \quad (5.8)$$

5.1 Coupled Operator Equations

We work in the Heisenberg-Langevin picture and assume that the pumping field is independent of z, and convert Eq.(7) from E-field to operator notation b_i . So that the right hand

side of each of Eqs.(7) is the same, we take $E_i \sim \sqrt{\omega_i \eta_i / \cos(\theta_i)} b_i$. The coupled operator equations for the Fourier components are then

$$\begin{aligned}\frac{\partial b_s}{\partial z} + \frac{\alpha_s}{\cos \theta_s} b_s &= \kappa b_i^\dagger \exp[i\Delta k_z z] + \sqrt{\frac{2\alpha_s}{\cos \theta_s}} f_s, \\ \frac{\partial b_i^\dagger}{\partial z} + \frac{\alpha_i}{\cos \theta_i} b_i^\dagger &= \kappa^* b_s \exp[-i\Delta k_z z] + \sqrt{\frac{2\alpha_i}{\cos \theta_i}} f_i^\dagger.\end{aligned}\quad (5.9)$$

Here, with $r = 1/\sqrt{\cos(\theta_s)\cos(\theta_i)\cos(\theta_p)}$, the coupling coefficient is $\kappa = \frac{r\zeta}{2}\sqrt{\omega_s\omega_i\omega_p\eta_s\eta_i\eta_p}$. Before proceeding with the solution, we transform Eqs (9) to constant coefficients by $b_s = a_s \exp(i\Delta k_z z/2)$ and $b_i^\dagger = a_i^\dagger \exp(-i\Delta k_z z/2)$. We then have

$$\begin{aligned}\frac{\partial a_s}{\partial z} + \left(\frac{\alpha_s}{\cos \theta_s} + i\frac{\Delta k_z}{2}\right) a_s &= \kappa a_i^\dagger + \sqrt{\frac{2\alpha_s}{\cos \theta_s}} f_s, \\ \frac{\partial a_i^\dagger}{\partial z} + \left(\frac{\alpha_i}{\cos \theta_i} - i\frac{\Delta k_z}{2}\right) a_i^\dagger &= \kappa^* a_s + \sqrt{\frac{2\alpha_i}{\cos \theta_i}} f_i^\dagger\end{aligned}\quad (5.10)$$

The operators $a(z, \mathbf{q}, \omega)$ are the coarse grained annihilation operators with commutator

$$[a_j(z_1, \mathbf{q}_1, \omega_1), a_k^\dagger(z_2, \mathbf{q}_2, \omega_2)] = \frac{1}{(2\pi)^3} \delta(z_1 - z_2) \delta(\mathbf{q}_1 - \mathbf{q}_2) \delta(\omega_1 - \omega_2). \quad (5.11)$$

They are normalized so that the signal and idler count rates per area are $\langle a_s^\dagger(\mathbf{r}, t) a_s(\mathbf{r}, t) \rangle$ and $\langle a_i^\dagger(\mathbf{r}, t) a_i(\mathbf{r}, t) \rangle$ respectively. The $f_s(z, \mathbf{q}, \omega)$ and $f_i^\dagger(z, \mathbf{q}, \omega)$ are the Langevin noise operators, and satisfy

$$[f_j(z, \mathbf{q}, \omega), f_k^\dagger(z', \mathbf{q}', \omega')] = \frac{1}{(2\pi)^3} \delta_{j,k} \delta(z - z') \delta(\mathbf{q} - \mathbf{q}') \delta(\omega - \omega'). \quad (5.12)$$

We have shown numerically that the commutator, Eq.(11) is conserved for all z . If the loss at both the signal and idler frequencies is zero, then the Langevin terms may be taken as zero, while still preserving the commutator. But when the loss is not zero these terms are essential for obtaining the correct generation rates at the signal and idler, as well as the coincidence count rate.

5.2 Solution

With L as the crystal length we write the solution of Eq. (10) in terms of a matrix \bar{M} and the exponential of this matrix $\exp(-\bar{M}L)$

$$\bar{M} = \begin{pmatrix} \alpha_s + i\Delta k_z/2 & \kappa \\ \kappa & \alpha_i - i\Delta k_z/2 \end{pmatrix}$$

and

$$\exp(-\bar{M}L) = \begin{pmatrix} A & B \\ C & D \end{pmatrix} \quad (5.13)$$

The solution of Eq. (10) is

$$\begin{bmatrix} a_s(L) \\ a_i^\dagger(L) \end{bmatrix} = \exp(-\bar{M}L) \begin{bmatrix} a_s(0) \\ a_i^\dagger(0) \end{bmatrix} + \int_0^L \exp(-\bar{M}(s-L)) \begin{bmatrix} f_s(s) \\ f_i^\dagger(s) \end{bmatrix} ds \quad (5.14)$$

Expanding

$$\begin{aligned} a_s(L) &= Aa_s(0) + Ba_i^\dagger(0) + \int_0^L E(s)f_s(s)ds + \int_0^L F(s)f_i^\dagger(s)ds \\ a_i^\dagger(L) &= Ca_s(0) + Da_i^\dagger(0) + \int_0^L G(s)f_s(s)ds + \int_0^L H(s)f_i^\dagger(s)ds \end{aligned} \quad (5.15)$$

where

$$\begin{aligned} E(s) &= \sqrt{2\alpha_s} \begin{bmatrix} 1 & 0 \end{bmatrix} \cdot \exp[\bar{M}(s-L)] \cdot \begin{bmatrix} 1 \\ 0 \end{bmatrix} \\ F(s) &= \sqrt{2\alpha_i} \begin{bmatrix} 1 & 0 \end{bmatrix} \cdot \exp[\bar{M}(s-L)] \cdot \begin{bmatrix} 0 \\ 1 \end{bmatrix} \\ G(s) &= \sqrt{2\alpha_s} \begin{bmatrix} 0 & 1 \end{bmatrix} \cdot \exp[\bar{M}(s-L)] \cdot \begin{bmatrix} 1 \\ 0 \end{bmatrix} \\ H(s) &= \sqrt{2\alpha_i} \begin{bmatrix} 0 & 1 \end{bmatrix} \cdot \exp[\bar{M}(s-L)] \cdot \begin{bmatrix} 0 \\ 1 \end{bmatrix} \end{aligned} \quad (5.16)$$

5.3 Signal and idler count rates

The quantities of interest, that is the generation rates, coincidence rates, and the temporal and spatial correlation functions may all be written in terms of the frequency domain functions that are defined in Eqs(15) and (16). The rate R_s [photons/(sec area)] of generation of signal photons is given by $R_s = \langle a_s^\dagger(\mathbf{r}, t)a_s(\mathbf{r}, t) \rangle$. We Fourier transform from $t \rightarrow \omega$, $x \rightarrow k_x$, and $y \rightarrow k_y$, and use Eq.(15) and Eq.(16), as well as the commutators of Eq.(11) and Eq.(12). With some algebra one obtains

$$\langle a_s^\dagger(t, \mathbf{r})a_s(t, \mathbf{r}) \rangle = \frac{1}{(2\pi)^3} \int_{\omega} \int_{\mathbf{q}} |B|^2 d\omega d\mathbf{q} + \frac{1}{(2\pi)^3} \int_{\omega} \int_{\mathbf{q}} \int_0^L |F(s)|^2 d\omega d\mathbf{q} ds \quad (5.17)$$

Similarly, the generation rate R_i [photons/(sec area)] at the idler wavelength is

$$\langle a_i^\dagger(t, \mathbf{r})a_i(t, \mathbf{r}) \rangle = \frac{1}{(2\pi)^3} \int_{\omega} \int_{\mathbf{q}} |C|^2 d\omega d\mathbf{q} + \frac{1}{(2\pi)^3} \int_{\omega} \int_{\mathbf{q}} \int_0^L |G(s)|^2 d\omega d\mathbf{q} ds \quad (5.18)$$

Because of the loss, the generation rate at the signal, may or may not, be equal to that at the idler wavelength. We assume a plane wave pump beam with a projected area on the x-y plane A_p ; so that the total count rate at either the signal or the idler is obtained by multiplying by A_p . But note, that since the square of the coupling coefficient in Eq. (10) is inversely proportional to A_p , the total generated count rate is independent of this area.

From their definitions in Eq.(15) we see that when the loss at the signal frequency is equal to zero, the quantity $|A|^2 = |A(\omega, k_x, k_y)|^2$ is the power gain G_s at the signal wavelength. The standard quantum limit requires that the count rate at the signal, i.e., the noise per temporal and angular bandwidth at the signal frequency, be equal to $G_s(\omega) - 1$. With the noise given by Eq.(17), we require that when $\alpha_s = 0$,

$$|A|^2 - 1 = |B|^2 + \int_0^L |F(s)|^2 ds \quad (5.19)$$

Similarly, when $\alpha_i = 0$,

$$|D|^2 - 1 = |C|^2 + \int_0^L |G(s)|^2 ds \quad (5.20)$$

We have numerically verified that the quantities A.....H satisfy Eqs.(19) and (20).

5.4 Correlations and coincidence counts

Assuming two ideal detectors each with an area A that is larger than that of the pumping beam, then if the first detector clicks at time t_1 and position $\mathbf{r}_1 = \{x_1, y_1\}$, the probability of the second detector clicking at time $t_2 = t_1 + \tau$ and position $\mathbf{r}_2 = \mathbf{r}_1 + \mu$, is given by the Glauber correlation function $G^{(2)}$

$$G^{(2)}(\tau, \mu) = \langle a_s^\dagger(t_2, \mathbf{r}_2) a_i^\dagger(t_1, \mathbf{r}_1) a_i(t_1, \mathbf{r}_1) a_s(t_2, \mathbf{r}_2) \rangle \quad (5.21)$$

To evaluate $G^{(2)}(\tau, \mu)$, we Fourier transform, use Wick's theorem, Eqs. (15) and (16) and the commutators of Eqs (11) and (12). With $\mathbf{q} = \{k_x, k_y\}$, it is useful to form the Fourier domain function

$$\phi(\omega, \mathbf{q}) = B^* D + \int_0^L F^*(s) H(s) ds \quad (5.22)$$

With considerable algebra we obtain

$$G^2(\tau) = \left(\frac{1}{2\pi} \right)^4 \int_{\mathbf{q}} \left| \int_{\omega} \phi(\omega, \mathbf{q}) \exp(i\omega\tau) d\omega \right|^2 d\mathbf{q} + R_s R_i \quad (5.23)$$

The background (or accidental coincidence count rate $R_s R_i$ is the result of signal and idler counts that accidentally arrive within the same temporal window. Most often it is small as compared to the first term. The coincidence count rate per area [photons/(sec area)] is

$$\int G(\tau) d\tau = \left(\frac{1}{2\pi} \right)^3 \int_{\omega} \int_{\mathbf{q}} |\phi(\omega, \mathbf{q})|^2 d\omega d\mathbf{q} \quad (5.24)$$

We may also evaluate the spatial correlation of the incident photons. For example if $x_2 = x_1 + \mu$, then with $\phi = \phi(\omega, k_x, k_y)$,

$$G^2(\mu) = \left(\frac{1}{2\pi} \right)^4 \int_{\omega} \int_{k_y} \left| \int_{k_x} \phi \exp(-ik_x x) dk_x \right|^2 dk_y d\omega \quad (5.25)$$

As a result of the much wider angular aperture in the out of plane dimension y , the correlation distance in this direction will be much narrower than in the in-plane dimension.

5.5 Δk_z in the Laue geometry

In the Laue geometry as described here, the input and output planes of the diamond crystal are normal to the z-axis and the monochromatic pump is in the x-z plane. We phase match using the (220) atomic planes with the reciprocal lattice k vector \vec{G} in the direction of the x-axis. Denoting the magnitude of the k-vectors of the signal, idler and pump as k_s , k_i , and k_p , the magnitude of the Bragg angle θ_B is $\arcsin(G/2k_p)$. The monochromatic pump propagates in the x-z plane at angle $\theta_p = -(\theta_B + \Delta)$, where Δ is most often less than a few mr. The phase matching angles of the signal θ_s and the idler θ_i are also in the x-z plane and are determined by the solution of $\vec{k}_s + \vec{k}_i = \vec{k}_p + \vec{G}$. For example, for a pump at 18 Kev the magnitude of the Bragg angle is .276 radians. For $\Delta = 1$ mr, $\theta_p = -.277$ radians, $\theta_s = .244$ and $\theta_i = .308$ radians, respectively.

With the phase matching angles of the central rays determined and denoted by θ_s and θ_i , we define $k_{pz0} = k_p \cos(\theta_p)$, $k_{sx0} = k_s \sin(\theta_s)$ and $k_{ix0} = k_i \sin(\theta_i)$; we take $k_{sy0} = k_{iy0} = 0$ and require that the sum of the tangential k-vectors in the x-y plane is zero. (For example, $k_{px} + k_{sx} + k_{ix} + G = 0$.) Noting that $k_{pz0} = k_{sz0} + k_{iz0}$, the k-vector mismatch in the z-direction is then

$$\Delta k_z = k_{pz0} - \sqrt{k_s^2 - k_{sx}^2 - k_{sy}^2} - \sqrt{k_i^2 - (k_{sx0} + k_{ix0} - k_{sx})^2 - k_{sy}^2} \quad (5.26)$$

When $k_{sx} = k_{sx0}$, and $k_{ix} = k_{ix0}$, then $\Delta k_z = 0$. With the group velocity at the signal and idler defined as V_s and V_i , then to lowest order in $\delta\omega_s = \omega_s - \omega_{s0}$, and $\delta k_{sx} = k_{sx} - k_{sx0}$, the quantity Δk_z expands to

$$\Delta k_z = [\sec(\theta_i)/V_i - \sec(\theta_s)/V_s]\delta\omega_s + [\tan(\theta_s) - \tan(\theta_i)]\delta k_{sx} + \frac{k_p \sec(\theta_s) \sec(\theta_i)}{k_s k_i} k_{sy}^2 \quad (5.27)$$

6 Appendix: Cavity-Enhanced SPDC

This appendix describes the theory associated with the experimental paper ‘‘A miniature ultrabright source of temporally long, narrowband biphotons’’, and was written by Chih-Sung Chuu.

6.1 Nonlinear Polarizations

The real generated polarizations for the signal and idler fields are

$$\begin{aligned}\hat{P}_s(z, t) &= \epsilon_0 \chi^{(2)} [\hat{E}_p(z, t) + \hat{E}_i(z, t)]^2 \\ \hat{P}_i(z, t) &= \epsilon_0 \chi^{(2)} [\hat{E}_p(z, t) + \hat{E}_s(z, t)]^2\end{aligned}\quad (6.1)$$

where $\hat{E}_p(z, t)$, $\hat{E}_s(z, t)$, and $\hat{E}_i(z, t)$ are also real numbers.

We write the traveling-wave pump field as

$$\hat{E}_p(z, t) = \frac{E_p(z, t)}{2} \exp[i(k_p z - \omega_p t)] + \text{c.c.} \quad (6.2)$$

where $E_p(z, t)$ is slowly-varying envelope, and approximate the standing-wave signal and idler fields by

$$\begin{aligned}\hat{E}_s(z, t) &= \frac{E_s(t)}{2} \sin \frac{q\pi z}{L} \exp(-i\omega_{s0}t) + \text{c.c.} \\ &= -\frac{iE_s(t)}{4} [\exp(i\frac{q\pi z}{L}) - \exp(-i\frac{q\pi z}{L})] \exp(-i\omega_{s0}t) + \text{c.c.} \\ \hat{E}_i(z, t) &= \frac{E_i(t)}{2} \sin \frac{r\pi z}{L} \exp(-i\omega_{i0}t) + \text{c.c.} \\ &= -\frac{iE_i(t)}{4} [\exp(i\frac{r\pi z}{L}) - \exp(-i\frac{r\pi z}{L})] \exp(-i\omega_{i0}t) + \text{c.c.}\end{aligned}\quad (6.3)$$

where q and r are integers corresponding to the cold cavity resonant frequencies $\Omega_q = q\pi c/n_s^{(g)}L$ and $\Omega_r = r\pi c/n_i^{(g)}L$, respectively, with $n_s^{(g)}$ and $n_i^{(g)}$ being the group indices of the signal and idler fields and L being the cavity length. $\omega_{s0} = \frac{1}{2}(\omega_p + \Omega_q - \Omega_r)$ and $\omega_{i0} = \frac{1}{2}(\omega_p - \Omega_q + \Omega_r)$ are the central frequencies of the signal and idler fields, which are near Ω_q and Ω_r , respectively, and satisfy the energy conservation, $\omega_p = \omega_{s0} + \omega_{i0}$.

Substituting the expressions of $\hat{E}_s(z, t)$, $\hat{E}_i(z, t)$ and $\hat{E}_p(z, t)$ into $\hat{P}_s(z, t)$ and $\hat{P}_i(z, t)$, we then obtain

$$\begin{aligned}
\hat{P}_s(z, t) &= \epsilon_0 \chi^{(2)} \left\{ \frac{E_p(z, t)}{2} \exp[i(k_p z - \omega_p t)] - \frac{iE_i(t)}{4} [\exp(i\frac{r\pi z}{L}) - \exp(-i\frac{r\pi z}{L})] \exp(-i\omega_{i0}t) + \text{c.c.} \right\}^2 \\
\hat{P}_i(z, t) &= \epsilon_0 \chi^{(2)} \left\{ \frac{E_p(z, t)}{2} \exp[i(k_p z - \omega_p t)] - \frac{iE_s(t)}{4} [\exp(i\frac{q\pi z}{L}) - \exp(-i\frac{q\pi z}{L})] \exp(-i\omega_{s0}t) + \text{c.c.} \right\}^2
\end{aligned}
\tag{6.4}$$

We keep the terms in $\hat{P}_s(z, t)$ and $\hat{P}_i(z, t)$ that have frequencies of ω_{s0} and ω_{i0} , respectively, with the signal and idler fields propagating in the same direction as the pump,

$$\begin{aligned}
\hat{P}_s(z, t) &= \frac{i\epsilon_0 \chi^{(2)}}{4} E_i^*(t) E_p(z, t) \exp[i(k_p - \frac{r\pi}{L})z - i\omega_{s0}t] + \text{c.c.} \\
\hat{P}_i(z, t) &= \frac{i\epsilon_0 \chi^{(2)}}{4} E_s^*(t) E_p(z, t) \exp[i(k_p - \frac{q\pi}{L})z - i\omega_{i0}t] + \text{c.c.}
\end{aligned}
\tag{6.5}$$

Since only the components that are nonorthogonal to $\sin(q\pi z/L)$ or $\sin(r\pi z/L)$ interact with the signal or idler fields, we project the polarizations against the corresponding spatial modes,

$$\begin{aligned}
\hat{P}_{s,q}(t) &= \frac{2}{L} \int_0^L \hat{P}_s(z, t) \sin(\frac{q\pi z}{L}) dz \\
\hat{P}_{i,r}(t) &= \frac{2}{L} \int_0^L \hat{P}_i(z, t) \sin(\frac{r\pi z}{L}) dz
\end{aligned}
\tag{6.6}$$

For $E_p(z, t) = E_p(t)$, the projected polarization at the signal frequency is

$$\begin{aligned}
\hat{P}_{s,q}(t) &= \frac{2}{L} \int_0^L \frac{i\epsilon_0\chi^{(2)}}{4} E_i^*(t)E_p(t) \exp[i(k_p - \frac{r\pi}{L})z - i\omega_{s0}t] \sin(\frac{q\pi z}{L}) dz + \text{c.c.} \\
&= \frac{i\epsilon_0\chi^{(2)}}{2L} E_i^*(t)E_p(t) \exp(-i\omega_{s0}t) \int_0^L \exp[i(k_p - \frac{r\pi}{L})z] \frac{\exp(i\frac{q\pi z}{L}) - \exp(-i\frac{q\pi z}{L})}{2i} dz + \text{c.c.} \\
&= \frac{\epsilon_0\chi^{(2)}}{4} \left\{ \frac{\exp[i(k_p - \frac{r\pi}{L} + \frac{q\pi}{L})L] - 1}{i(k_p - \frac{r\pi}{L} + \frac{q\pi}{L})L} - \frac{\exp[i(k_p - \frac{r\pi}{L} - \frac{q\pi}{L})L] - 1}{i(k_p - \frac{r\pi}{L} - \frac{q\pi}{L})L} \right\} E_i^*(t)E_p(t) \exp(-i\omega_{s0}t) + \text{c.c.} \\
&= \frac{\epsilon_0\chi^{(2)}}{4} \left\{ -\frac{\exp[i(k_p - \frac{r\pi}{L} - \frac{q\pi}{L})L] - 1}{i(k_p - \frac{r\pi}{L} - \frac{q\pi}{L})L} \right\} E_i^*(t)E_p(t) \exp(-i\omega_{s0}t) + \text{c.c.} \tag{6.7}
\end{aligned}$$

where, in the last equality, we only keep the term in which the signal propagates in the same direction as the pump. Defining

$$\Delta k = k_p - \frac{r\pi}{L} - \frac{q\pi}{L} \tag{6.8}$$

the projected polarization at the signal frequency can be written as

$$\begin{aligned}
\hat{P}_{s,q}(t) &= i\frac{\epsilon_0\chi^{(2)}}{4} \left[\frac{\exp(i\Delta kL) - 1}{\Delta kL} \right] E_i^*(t)E_p(t) \exp(-i\omega_{s0}t) + \text{c.c.} \\
&= \frac{P_{s,q}(t)}{2} \exp(-i\omega_{s0}t) + \text{c.c.} \tag{6.9}
\end{aligned}$$

where the slowly-varying envelope

$$P_{s,q}(t) = -\frac{\epsilon_0\chi^{(2)}}{2} \exp(i\Delta kL/2) \text{sinc}(\Delta kL/2) E_i^*(t)E_p(t) \tag{6.10}$$

Similarly, the projected polarization at the idler frequency is

$$\begin{aligned}
\hat{P}_{i,r}(t) &= -\frac{\epsilon_0\chi^{(2)}}{4} \exp(i\Delta kL/2) \text{sinc}(\Delta kL/2) E_s^*(t)E_p(t) \exp(-i\omega_{i0}t) + \text{c.c.} \\
&= \frac{P_{i,r}(t)}{2} \exp(-i\omega_{i0}t) + \text{c.c.} \tag{6.11}
\end{aligned}$$

where the slowly-varying envelope

$$P_{i,r}(t) = -\frac{\epsilon_0\chi^{(2)}}{2} \exp(i\Delta kL/2) \text{sinc}(\Delta kL/2) E_s^*(t)E_p(t) \tag{6.12}$$

6.2 SVEA (Lamb) Equations

Defining $\hat{E}_s(t)$ and $\hat{E}_i(t)$ as

$$\begin{aligned}\hat{E}_s(z, t) &= \hat{E}_s(t) \sin\left(\frac{q\pi z}{L}\right) \\ \hat{E}_i(z, t) &= \hat{E}_i(t) \sin\left(\frac{r\pi z}{L}\right)\end{aligned}\tag{6.13}$$

the second-order differential equation for $\hat{E}_s(t)$ and $\hat{P}_{s,q}(t)$ is given by

$$\frac{\partial^2 \hat{E}_s(t)}{\partial t^2} + \frac{\Omega_q}{Q_s} \frac{\partial \hat{E}_s(t)}{\partial t} + \Omega_q^2 \hat{E}_s(t) = -\frac{1}{\epsilon_o \epsilon_s} \frac{\partial^2 \hat{P}_{s,q}(t)}{\partial t^2}\tag{6.14}$$

where $Q_s = \epsilon_o \epsilon_s \Omega_q / \sigma_s$ is the cavity quality factor.

Substituting,

$$\begin{aligned}\hat{P}_s(t) &= \frac{P_s(t)}{2} \exp(-i\omega_{s0}t) + \text{c.c.} \\ \hat{E}_s(t) &= \frac{E_s(t)}{2} \exp(-i\omega_{s0}t) + \text{c.c.}\end{aligned}\tag{6.15}$$

into the second-order differential equation and picking out the $e^{-i\omega_{s0}t}$ terms, we have

$$\frac{\partial^2 E_s(t)}{\partial t^2} + \left(\frac{\Omega_q}{Q_s} - 2i\omega_{s0}\right) \frac{\partial E_s(t)}{\partial t} + (\Omega_q^2 - \omega_{s0}^2 - i\frac{\Omega_q}{Q_s} \omega_{s0}) E_s(t) = -\frac{1}{\epsilon_o \epsilon_s} \left[\frac{\partial^2 P_{s,q}(t)}{\partial t^2} - 2i\omega_{s0} \frac{\partial P_{s,q}(t)}{\partial t} - \omega_{s0}^2 P_{s,q}(t) \right]\tag{6.16}$$

The slowly-varying envelope approximations assumes that

$$\frac{\partial^2}{\partial t^2} \ll \omega_{s0} \frac{\partial}{\partial t} \ll \omega_{s0}^2\tag{6.17}$$

Furthermore, since $\omega_{s0} \approx \Omega_q$,

$$\Omega_q^2 - \omega_{s0}^2 = (\Omega_q + \omega_{s0})(\Omega_q - \omega_{s0}) \approx 2\omega_{s0}(\Omega_q - \omega_{s0}) \quad (6.18)$$

We also assume that the cavity decay rate is small compared to the resonant frequency of the cavity

$$\Gamma_s = \frac{\Omega_q}{Q_s} \ll \Omega_q \quad (6.19)$$

With these approximations, we obtain the complex SVEA equation

$$\frac{\partial E_s(t)}{\partial t} + \left[i(\Omega_q - \omega_{s0}) + \frac{\Omega_q}{2Q_s} \right] E_s(t) = \frac{i\omega_{s0}}{2\epsilon_o\epsilon_s} P_{s,q}(t) \quad (6.20)$$

Similarly, for $E_i(t)$ and $P_{i,r}$, we have

$$\frac{\partial E_i(t)}{\partial t} + \left[i(\Omega_r - \omega_{i0}) + \frac{\Omega_r}{2Q_i} \right] E_i(t) = \frac{i\omega_{i0}}{2\epsilon_o\epsilon_i} P_{i,r}(t) \quad (6.21)$$

where $Q_i = \epsilon_o\epsilon_i\Omega_r/\sigma_i$.

Substituting the explicit forms of $P_{s,q}(t)$ and $P_{i,r}(t)$ into the SVEA equations, we obtain the coupled SVEA equations,

$$\begin{aligned} \frac{\partial E_s(t)}{\partial t} + \left[i(\Omega_q - \omega_{s0}) + \frac{\Omega_q}{2Q_s} \right] E_s(t) &= -\frac{i\omega_{s0}\chi^{(2)}}{4\epsilon_s} \exp(i\Delta kL/2) \operatorname{sinc}(\Delta kL/2) E_i^*(t) E_p(t) \\ \frac{\partial E_i(t)}{\partial t} + \left[i(\Omega_r - \omega_{i0}) + \frac{\Omega_r}{2Q_i} \right] E_i(t) &= -\frac{i\omega_{i0}\chi^{(2)}}{4\epsilon_i} \exp(i\Delta kL/2) \operatorname{sinc}(\Delta kL/2) E_s^*(t) E_p(t) \end{aligned} \quad (6.22)$$

6.3 Standing Wave

To quantize a standing-wave field,

$$E_{st}(z, t) = E_{st}(t) \sin \frac{m\pi z}{L} \quad (6.23)$$

we note that the energy per area stored in cavity

$$W(t) = \frac{1}{4} \epsilon_0 \epsilon L |E_{st}(t)|^2 \quad (6.24)$$

where L is the cavity length, is equal to the energy per area of the photon,

$$W(t) = \hbar \omega_{st} |a_{st}(t)|^2 \quad (6.25)$$

where ω_{st} is the angular frequency of the photon and $a_{st}(t)$ is the annihilation operator of the photon with units of (photon number/area)^{1/2}. The conversion from $E_{st}(t)$ to $a_{st}(t)$ is then

$$E_{st}(t) = 2 \sqrt{\frac{\hbar \omega_{st}}{\epsilon_0 \epsilon_{st} L}} a_{st}(t) \quad (6.26)$$

For $E_{st}^*(t)$ and $a_{st}^\dagger(t)$, the conversion is

$$E_{st}^*(t) = 2 \sqrt{\frac{\hbar \omega_{st}}{\epsilon_0 \epsilon_{st} L}} a_{st}^\dagger(t) \quad (6.27)$$

6.4 Traveling Wave

For a traveling wave $E_t(t)$, the power per unit area is

$$I_t(t) = \frac{1}{2\eta_t} |E_t(t)|^2 \quad (6.28)$$

which is equal to that of the photon field,

$$I_t(t) = \hbar\omega_t |a_t(t)|^2 \quad (6.29)$$

where $a_t(t)$ is the annihilation operator of the photon field and has units of (photon number/time/area)^{1/2}. The conversion between $E_t(t)$ and $a_t(t)$ is then

$$E_t(t) = \sqrt{2\hbar\omega_t\eta_t} a_t(t) \quad (6.30)$$

For $E_t^*(t)$ and $a_t^\dagger(t)$, it is

$$E_t^*(t) = \sqrt{2\hbar\omega_t\eta_t} a_t^\dagger(t) \quad (6.31)$$

6.5 Quantized coupled SVEA (Lamb) Equations

The coupled SVEA equations are

$$\begin{aligned} \frac{\partial E_s(t)}{\partial t} + \left[i(\Omega_q - \omega_{s0}) + \frac{\Omega_q}{2Q_s} \right] E_s(t) &= -\frac{i\omega_{s0}\chi^{(2)}}{4\epsilon_s} \exp(i\Delta kL/2) \operatorname{sinc}(\Delta kL/2) E_i^*(t) E_p(t) \\ \frac{\partial E_i(t)}{\partial t} + \left[i(\Omega_r - \omega_{i0}) + \frac{\Omega_r}{2Q_i} \right] E_i(t) &= -\frac{i\omega_{i0}\chi^{(2)}}{4\epsilon_i} \exp(i\Delta kL/2) \operatorname{sinc}(\Delta kL/2) E_s^*(t) E_p(t) \end{aligned} \quad (6.32)$$

Using the field normalizations and noting that $\eta_{s,i} = \eta_0/n_{s,i}$, $\epsilon_{s,i} = n_{s,i}^2$, and $c = 1/\epsilon_0\eta_0$, we obtain the quantized coupled SVEA equations,

$$\begin{aligned} \frac{\partial a_s(t)}{\partial t} + \left[i(\Omega_q - \omega_{s0}) + \frac{\Gamma_s}{2} \right] a_s(t) &= -i\kappa a_i^\dagger(t) + \sqrt{\gamma_s} b_s^{\text{in}}(t) \\ \frac{\partial a_i(t)}{\partial t} + \left[i(\Omega_r - \omega_{i0}) + \frac{\Gamma_i}{2} \right] a_i(t) &= -i\kappa a_s^\dagger(t) + \sqrt{\gamma_i} b_i^{\text{in}}(t) \\ b_s^{\text{out}}(t) &= \sqrt{\gamma_s} a_s(t) - b_s^{\text{in}}(t) \\ b_i^{\text{out}}(t) &= \sqrt{\gamma_i} a_i(t) - b_i^{\text{in}}(t) \end{aligned} \quad (6.33)$$

where $b_{s,i}^{\text{in}}(t)$ and $b_{s,i}^{\text{out}}(t)$ are the annihilation operators of the input and output coupling fields (traveling wave) at the output mirror, respectively, and have units of (photon number/area/time)^{1/2}. $\Gamma_{s,i} = \Omega_{q,r}/Q_{s,i} = \Delta_{s,i}[2\xi_{s,i} + (1 - r_{s,i})]$ are the total power decay rates with $\Delta_{s,i}$ being the free spectral ranges, $r_{s,i}$ being the reflectivities of mirrors, and $\xi_{s,i}$ being the absorption losses of crystal per trip, and $\gamma_{s,i} = \Delta_{s,i}(1 - r_{s,i})$ are the power decay rates due to the coupling. $\kappa = \kappa_0 \exp(i\Delta kL/2) \text{sinc}(\Delta kL/2)$ with $\kappa_0 = \frac{1}{2} d\epsilon_0^2 c^2 \eta_s \eta_i (\omega_s \omega_i)^{1/2} E_p$, where $d = \chi^{(2)}/2$, ω_s and ω_i are the oscillation frequencies of the signal and idler fields, respectively, and $\omega_{s0} \approx \omega_s$ and $\omega_{i0} \approx \omega_i$ are used.

6.6 Power Conservation

We first consider the case where there is no pump, $E_p = 0$, and therefore $\kappa = 0$. The coupled equations become

$$\begin{aligned} \frac{\partial a_s(t)}{\partial t} + \frac{\Gamma'_s}{2} a_s(t) &= \sqrt{\gamma_s} b_s^{\text{in}}(t) \\ \frac{\partial a_i(t)}{\partial t} + \frac{\Gamma'_i}{2} a_i(t) &= \sqrt{\gamma_i} b_i^{\text{in}}(t) \end{aligned} \quad (6.34)$$

where $\Gamma'_s = i2(\Omega_q - \omega_{s0}) + \Gamma_s$ and $\Gamma'_i = i2(\Omega_r - \omega_{i0}) + \Gamma_i$.

To calculate the photon rate per area of the signal field inside the cavity,

$$\frac{\partial |a_s(t)|^2}{\partial t} = a_s^\dagger(t) \frac{\partial a_s(t)}{\partial t} + a_s(t) \frac{\partial a_s^\dagger(t)}{\partial t} \quad (6.35)$$

we note that

$$\begin{aligned} a_s^\dagger(t) \frac{\partial a_s(t)}{\partial t} &= \frac{b_s^{\text{out}\dagger}(t) + b_s^{\text{in}\dagger}(t)}{\sqrt{\gamma_s}} \left[\sqrt{\gamma_s} b_s^{\text{in}}(t) - \frac{\Gamma'_s}{2} a_s(t) \right] \\ &= [b_s^{\text{out}\dagger}(t) + b_s^{\text{in}\dagger}(t)] b_s^{\text{in}}(t) - \left[\frac{b_s^{\text{out}\dagger}(t) + b_s^{\text{in}\dagger}(t)}{\sqrt{\gamma_s}} \right] \frac{\Gamma'_s}{2} \left[\frac{b_s^{\text{out}}(t) + b_s^{\text{in}}(t)}{\sqrt{\gamma_s}} \right] \\ &= \left(1 - \frac{\Gamma'_s}{2\gamma_s} \right) |b_s^{\text{in}}(t)|^2 - \frac{\Gamma'_s}{2\gamma_s} |b_s^{\text{out}}(t)|^2 + \left(1 - \frac{\Gamma'_s}{2\gamma_s} \right) b_s^{\text{out}\dagger}(t) b_s^{\text{in}}(t) - \frac{\Gamma'_s}{2\gamma_s} b_s^{\text{in}\dagger}(t) b_s^{\text{out}}(t) \end{aligned} \quad (6.36)$$

We hence have

$$\frac{\partial |a_s(t)|^2}{\partial t} = 2 \left(1 - \frac{\Gamma_s}{2\gamma_s}\right) |b_s^{\text{in}}(t)|^2 - \frac{\Gamma_s}{\gamma_s} |b_s^{\text{out}}(t)|^2 + \left(1 - \frac{\Gamma_s}{\gamma_s}\right) b_s^{\text{out}\dagger}(t) b_s^{\text{in}}(t) + \left(1 - \frac{\Gamma_s}{\gamma_s}\right) b_s^{\text{in}\dagger}(t) b_s^{\text{out}}(t) \quad (6.37)$$

where we use the commutator $[b^i(t'), b^j(t)] = \delta_{ij} \delta(t' - t)$.

For a lossless cavity, $\Gamma_s = \gamma_s$, we then have

$$\frac{\partial |a_s(t)|^2}{\partial t} = |b_s^{\text{in}}(t)|^2 - |b_s^{\text{out}}(t)|^2 \quad (6.38)$$

which says that the photon rate per area of the signal field inside the cavity equals to the difference of that of the input and output photons in the same cavity mode. Similarly, for the idler field,

$$\frac{\partial |a_i(t)|^2}{\partial t} = |b_i^{\text{in}}(t)|^2 - |b_i^{\text{out}}(t)|^2 \quad (6.39)$$

6.7 With Pump

We next consider the case where pump is present. We note that

$$\begin{aligned} a_s^\dagger(t) \frac{\partial a_s(t)}{\partial t} &= a_s^\dagger(t) \left[\sqrt{\gamma_s} b_s^{\text{in}}(t) - \frac{\Gamma'_s}{2} a_s(t) - i\kappa a_i^\dagger(t) \right] \\ &= a_s^\dagger(t) \left[\sqrt{\gamma_s} b_s^{\text{in}}(t) - \frac{\Gamma'_s}{2} a_s(t) \right] - i\kappa a_s^\dagger(t) a_i^\dagger(t) \end{aligned} \quad (6.40)$$

The photon rate per area of the signal field inside a lossless cavity is then

$$\frac{\partial |a_s(t)|^2}{\partial t} = |b_s^{\text{in}}(t)|^2 - |b_s^{\text{out}}(t)|^2 + [i\kappa^* a_s(t)a_i(t) - i\kappa a_s^\dagger(t)a_i^\dagger(t)] \quad (6.41)$$

Similarly, for the idler field, we have

$$\frac{\partial |a_i(t)|^2}{\partial t} = |b_i^{\text{in}}(t)|^2 - |b_i^{\text{out}}(t)|^2 + [i\kappa^* a_s(t)a_i(t) - i\kappa a_s^\dagger(t)a_i^\dagger(t)] \quad (6.42)$$

where we use the commutator $[a_j(t'), a_k(t)] = \delta_{jk}\delta(t' - t)$. Comparing the above two equations, we see that

$$\frac{\partial |a_s(t)|^2}{\partial t} + |b_s^{\text{out}}(t)|^2 - |b_s^{\text{in}}(t)|^2 = \left(\frac{\partial |a_i(t)|^2}{\partial t} + |b_i^{\text{out}}(t)|^2 - |b_i^{\text{in}}(t)|^2 \right) \quad (6.43)$$

6.8 Output Fields

The coupled SVEA equations in the time domain are

$$\begin{aligned} \frac{\partial a_s(t)}{\partial t} + \left[-i(\omega_{s0} - \Omega_q) + \frac{\Gamma_s}{2} \right] a_s(t) &= -i\kappa a_i^\dagger(t) + \sqrt{\gamma_s} b_s^{\text{in}}(t) \\ \frac{\partial a_i^\dagger(t)}{\partial t} + \left[i(\omega_{i0} - \Omega_r) + \frac{\Gamma_i}{2} \right] a_i^\dagger(t) &= i\kappa a_s(t) + \sqrt{\gamma_i} b_i^{\text{in}\dagger}(t) \end{aligned} \quad (6.44)$$

We will use the Fourier transform pairs,

$$\begin{aligned} f(t) &= \int_{-\infty}^{\infty} f(\delta\omega) \exp(-i\delta\omega t) d\delta\omega \\ f(\delta\omega) &= \frac{1}{2\pi} \int_{-\infty}^{\infty} f(t) \exp(i\delta\omega t) dt \end{aligned} \quad (6.45)$$

to obtain the coupled SVEA equations in the frequency domain, where $\delta\omega$ is a low-frequency variable that is relative to the carrier frequencies ω_{s0} or ω_{i0} . For the signal field, the Fourier transform pairs of the annihilation operator are

$$\begin{aligned}
a_s(t) &= \int_{-\infty}^{\infty} a_s(\omega - \omega_{s0}) \exp[-i(\omega - \omega_{s0})t] d(\omega - \omega_{s0}) \\
a_s(\omega - \omega_{s0}) &= \frac{1}{2\pi} \int_{-\infty}^{\infty} a_s(t) \exp[i(\omega - \omega_{s0})t] dt
\end{aligned} \tag{6.46}$$

where ω is the oscillation frequency of the signal field. For the idler field, the Fourier transform pairs of the annihilation operator are

$$\begin{aligned}
a_i(t) &= \int_{-\infty}^{\infty} a_i(\omega_i - \omega_{i0}) \exp[-i(\omega_i - \omega_{i0})t] d(\omega_i - \omega_{i0}) \\
a_i(\omega_i - \omega_{i0}) &= \frac{1}{2\pi} \int_{-\infty}^{\infty} a_i(t) \exp[i(\omega_i - \omega_{i0})t] dt
\end{aligned} \tag{6.47}$$

where $\omega_i = \omega_p - \omega$ is the oscillation frequency of the idler field.

Noting that

$$\begin{aligned}
\mathcal{F} [f^\dagger(t)] &= \frac{1}{2\pi} \int_{-\infty}^{\infty} f^\dagger(t) \exp(i\delta\omega t) dt = \left\{ \frac{1}{2\pi} \int_{-\infty}^{\infty} f(t) \exp[i(-\delta\omega)t] dt \right\}^\dagger = f^\dagger(-\delta\omega) \\
\mathcal{F} \left[\frac{\partial f(t)}{\partial t} \right] &= \frac{1}{2\pi} \int_{-\infty}^{\infty} \frac{\partial f(t)}{\partial t} \exp(i\delta\omega t) dt = \frac{1}{2\pi} \int_{-\infty}^{\infty} \left\{ \frac{\partial}{\partial t} f(t) \exp(i\delta\omega t) - i\delta\omega f(t) \exp(i\delta\omega t) \right\} dt \\
&= \frac{1}{2\pi} [f(t) \exp(i\delta\omega t)]_{-\infty}^{\infty} - i\delta\omega f(\delta\omega) = -i\delta\omega f(\delta\omega)
\end{aligned} \tag{6.48}$$

where we assume that $f(t)$ is bounded so that $f(t \rightarrow \pm\infty) = 0$, we obtain the Fourier-transformed coupled SVEA equations

$$\begin{aligned}
-i(\omega - \Omega_q) a_s(\omega - \omega_{s0}) + \frac{\Gamma_s}{2} a_s(\omega - \omega_{s0}) &= -i\kappa a_i^\dagger(-\omega_i + \omega_{i0}) + \sqrt{\gamma_s} b_s^{\text{in}}(\omega - \omega_{s0}) \\
i(\omega_i - \Omega_r) a_i^\dagger(-\omega_i + \omega_{i0}) + \frac{\Gamma_i}{2} a_i^\dagger(-\omega_i + \omega_{i0}) &= i\kappa a_s(\omega - \omega_{s0}) + \sqrt{\gamma_i} b_i^{\text{in}\dagger}(-\omega_i + \omega_{i0})
\end{aligned} \tag{6.49}$$

The operators in the coupled equations are slowly-varying envelopes. To convert them to rapidly-varying analytic signals, $\hat{a}_s(\omega)$, $\hat{a}_i(\omega_i)$, $\hat{b}_s(\omega)$, and $\hat{b}_i(\omega_i)$, we note that

$$\begin{aligned}\hat{a}_{s,i}(t) &= a_{s,i}(t) \exp(-i\omega_{s0,i0}t) \\ \hat{b}_{s,i}(t) &= b_{s,i}(t) \exp(-i\omega_{s0,i0}t)\end{aligned}\tag{6.50}$$

and therefore

$$\begin{aligned}a_{s,i}(\omega') &= \hat{a}_{s,i}(\omega' + \omega_{s0,i0}) \\ b_{s,i}(\omega') &= \hat{b}_{s,i}(\omega' + \omega_{s0,i0})\end{aligned}\tag{6.51}$$

The coupled SVEA equations for the rapidly-varying analytic signals are then

$$\begin{aligned}-i(\omega - \Omega_q) \hat{a}_s(\omega) + \frac{\Gamma_s}{2} \hat{a}_s(\omega) &= -i\kappa \hat{a}_i^\dagger(-\omega_i) + \sqrt{\gamma_s} \hat{b}_s^{\text{in}}(\omega) \\ i(\omega_i - \Omega_r) \hat{a}_i^\dagger(-\omega_i) + \frac{\Gamma_i}{2} \hat{a}_i^\dagger(-\omega_i) &= i\kappa \hat{a}_s(\omega) + \sqrt{\gamma_i} \hat{b}_i^{\text{in}\dagger}(-\omega_i)\end{aligned}\tag{6.52}$$

We rewrite the above equations in the matrix form,

$$\begin{pmatrix} -i(\omega - \Omega_q) + \frac{\Gamma_s}{2} & i\kappa \\ -i\kappa & i(\omega_i - \Omega_r) + \frac{\Gamma_i}{2} \end{pmatrix} \begin{pmatrix} \hat{a}_s(\omega) \\ \hat{a}_i^\dagger(-\omega_i) \end{pmatrix} = \begin{pmatrix} \sqrt{\gamma_s} \hat{b}_s^{\text{in}}(\omega) \\ \sqrt{\gamma_i} \hat{b}_i^{\text{in}\dagger}(-\omega_i) \end{pmatrix}\tag{6.53}$$

to obtain $\hat{a}_s(\omega)$ and $\hat{a}_i^\dagger(-\omega_i)$ in terms of $\hat{b}_s^{\text{in}}(\omega)$ and $\hat{b}_i^{\text{in}\dagger}(-\omega_i)$,

$$\begin{aligned}\begin{pmatrix} \hat{a}_s(\omega) \\ \hat{a}_i^\dagger(-\omega_i) \end{pmatrix} &= \begin{pmatrix} -i(\omega - \Omega_q) + \frac{\Gamma_s}{2} & i\kappa \\ -i\kappa & i(\omega_i - \Omega_r) + \frac{\Gamma_i}{2} \end{pmatrix}^{-1} \begin{pmatrix} \sqrt{\gamma_s} \hat{b}_s^{\text{in}}(\omega) \\ \sqrt{\gamma_i} \hat{b}_i^{\text{in}\dagger}(-\omega_i) \end{pmatrix} \\ &= \frac{\begin{pmatrix} [i(\omega_i - \Omega_r) + \frac{\Gamma_i}{2}]\sqrt{\gamma_s} & -i\kappa\sqrt{\gamma_i} \\ i\kappa\sqrt{\gamma_s} & [-i(\omega - \Omega_q) + \frac{\Gamma_s}{2}]\sqrt{\gamma_i} \end{pmatrix}}{\begin{vmatrix} -i(\omega - \Omega_q) + \frac{\Gamma_s}{2} & i\kappa \\ -i\kappa & i(\omega_i - \Omega_r) + \frac{\Gamma_i}{2} \end{vmatrix}} \begin{pmatrix} \hat{b}_s^{\text{in}}(\omega) \\ \hat{b}_i^{\text{in}\dagger}(-\omega_i) \end{pmatrix}\end{aligned}\tag{6.54}$$

The slowly-varying output fields, $b_s^{\text{out}}(t)$ and $b_i^{\text{out}}(t)$, are related to the internal fields, $a_s(t)$ and $a_i(t)$, and the input fields, $b_s^{\text{in}}(t)$ and $b_i^{\text{in}}(t)$, through

$$\begin{pmatrix} b_s^{\text{out}}(t) \\ b_i^{\text{out}\dagger}(t) \end{pmatrix} = \begin{pmatrix} \sqrt{\gamma_s} & 0 \\ 0 & \sqrt{\gamma_i} \end{pmatrix} \begin{pmatrix} a_s(t) \\ a_i^\dagger(t) \end{pmatrix} - \begin{pmatrix} b_s^{\text{in}}(t) \\ b_i^{\text{in}\dagger}(t) \end{pmatrix} \quad (6.55)$$

Taking Fourier transform of these equations followed by conversion to rapidly-varying analytic signals, we have

$$\begin{pmatrix} \hat{b}_s^{\text{out}}(\omega) \\ \hat{b}_i^{\text{out}\dagger}(-\omega_i) \end{pmatrix} = \begin{pmatrix} \sqrt{\gamma_s} & 0 \\ 0 & \sqrt{\gamma_i} \end{pmatrix} \begin{pmatrix} \hat{a}_s(\omega) \\ \hat{a}_i^\dagger(-\omega_i) \end{pmatrix} - \begin{pmatrix} \hat{b}_s^{\text{in}}(\omega) \\ \hat{b}_i^{\text{in}\dagger}(-\omega_i) \end{pmatrix} = \begin{pmatrix} A(\omega) & B(\omega) \\ C(\omega) & D(\omega) \end{pmatrix} \begin{pmatrix} \hat{b}_s^{\text{in}}(\omega) \\ \hat{b}_i^{\text{in}\dagger}(-\omega_i) \end{pmatrix} \quad (6.56)$$

or

$$\begin{aligned} \hat{b}_s^{\text{out}}(\omega) &= A(\omega) \hat{b}_s^{\text{in}}(\omega) + B(\omega) \hat{b}_i^{\text{in}\dagger}(-\omega_i) \\ \hat{b}_i^{\text{out}\dagger}(-\omega_i) &= C(\omega) \hat{b}_s^{\text{in}}(\omega) + D(\omega) \hat{b}_i^{\text{in}\dagger}(-\omega_i) \end{aligned} \quad (6.57)$$

where

$$\begin{aligned} A(\omega) &= \frac{[\frac{\Gamma_i}{2} + i(\omega_i - \Omega_r)][\gamma_s - \frac{\Gamma_s}{2} + i(\omega - \Omega_q)] + \kappa^2}{[\frac{\Gamma_s}{2} - i(\omega - \Omega_q)][\frac{\Gamma_i}{2} + i(\omega_i - \Omega_r)] + \kappa^2} \\ B(\omega) &= \frac{-i\kappa\sqrt{\gamma_s\gamma_i}}{[\frac{\Gamma_s}{2} - i(\omega - \Omega_q)][\frac{\Gamma_i}{2} + i(\omega_i - \Omega_r)] - \kappa^2} \\ C(\omega) &= \frac{i\kappa\sqrt{\gamma_s\gamma_i}}{[\frac{\Gamma_s}{2} - i(\omega - \Omega_q)][\frac{\Gamma_i}{2} + i(\omega_i - \Omega_r)] - \kappa^2} \\ D(\omega) &= \frac{[\frac{\Gamma_s}{2} - i(\omega - \Omega_q)][\gamma_i - \frac{\Gamma_i}{2} - i(\omega_i - \Omega_r)] + \kappa^2}{[\frac{\Gamma_s}{2} - i(\omega - \Omega_q)][\frac{\Gamma_i}{2} + i(\omega_i - \Omega_r)] - \kappa^2} \end{aligned} \quad (6.58)$$

and $\omega_i = \omega_p - \omega$.

For a lossless cavity ($\gamma_s = \Gamma_s$, $\gamma_i = \Gamma_i$), $A(\omega)$, $B(\omega)$, $C(\omega)$, and $D(\omega)$ are related by the unitary conditions,

$$\begin{aligned}
A(\omega)C^*(\omega) &= B(\omega)D^*(\omega) \\
|A(\omega)|^2 - |B(\omega)|^2 &= 1 \\
|C(\omega)|^2 - |D(\omega)|^2 &= 1
\end{aligned} \tag{6.59}$$

6.9 Spatial Coupling Factor and Gaussian Beam

Before calculating the paired count rate and spectral Power spectral density, we will include the spatial coupling factors at confocal condition into κ .

The modified classical coupled SVEA equations read

$$\begin{aligned}
\frac{\partial E_s(t)}{\partial t} + \left[i(\Omega_q - \omega_{s0}) + \frac{\Omega_q}{2Q_s} \right] E_s(t) &= -g_s \frac{i\omega_{s0}\chi^{(2)}}{4\epsilon_s} \exp(i\Delta kL/2) \operatorname{sinc}(\Delta kL/2) E_i^*(t) E_p(t) \\
\frac{\partial E_i(t)}{\partial t} + \left[i(\Omega_r - \omega_{i0}) + \frac{\Omega_r}{2Q_i} \right] E_i(t) &= -g_i \frac{i\omega_{i0}\chi^{(2)}}{4\epsilon_i} \exp(i\Delta kL/2) \operatorname{sinc}(\Delta kL/2) E_s^*(t) E_p(t)
\end{aligned}$$

where the spatial coupling factors are

$$\begin{aligned}
g_s &= \frac{2W_p^2 W_i^2}{W_p^2 W_s^2 + W_p^2 W_i^2 + W_s^2 W_i^2} = \frac{2A_p A_i}{A_p A_s + A_p A_i + A_s A_i} \\
g_i &= \frac{2W_p^2 W_s^2}{W_p^2 W_i^2 + W_p^2 W_s^2 + W_s^2 W_i^2} = \frac{2A_p A_s}{A_p A_i + A_p A_s + A_s A_i}
\end{aligned} \tag{6.61}$$

with W_p , W_s , and W_i (defined below) being the $1/e^2$ beam radii of the pump, signal, and idler beams at the focus, respectively, and A_p , A_s , and A_i are the corresponding spot sizes.

When the cofocal length equals to the crystal length, spot sizes are the smallest

$$\begin{aligned}
A_p &= \pi \left(\frac{W_p}{\sqrt{2}} \right)^2 = \frac{\lambda_p L}{4n_p} \\
A_s &= \pi \left(\frac{W_s}{\sqrt{2}} \right)^2 = \frac{\lambda_s L}{4n_p} \\
A_i &= \pi \left(\frac{W_i}{\sqrt{2}} \right)^2 = \frac{\lambda_i L}{4n_i}
\end{aligned} \tag{6.62}$$

The field normalizations change accordingly to

$$\begin{aligned}
E_j(t) &= 2\sqrt{\frac{\hbar\omega_j}{\epsilon_0\epsilon_j LA_j}} a_j(t) \text{ for standing waves} \\
E_j(t) &= \sqrt{\frac{2\hbar\omega_j\eta_j}{A_j}} a_j(t) \text{ for traveling waves}
\end{aligned} \tag{6.63}$$

and $a_j(t)$ has unit of photon number for standing waves and photon number/s for traveling waves.

The quantized coupled SVEA equations have the same form,

$$\begin{aligned}
\frac{\partial a_s(t)}{\partial t} + \left[i(\Omega_q - \omega_{s0}) + \frac{\Gamma_s}{2} \right] a_s(t) &= -i\kappa a_i^\dagger(t) + \sqrt{\gamma_s} b_s^{\text{in}}(t) \\
\frac{\partial a_i(t)}{\partial t} + \left[i(\Omega_r - \omega_{i0}) + \frac{\Gamma_i}{2} \right] a_i(t) &= -i\kappa a_s^\dagger(t) + \sqrt{\gamma_i} b_i^{\text{in}}(t)
\end{aligned} \tag{6.64}$$

where $\kappa = \kappa_0 \exp(i\Delta kL/2)\text{sinc}(\Delta kL/2)$ with

$$\kappa_0 = \frac{1}{2} d\epsilon_0^2 c^2 \eta_s \eta_i (\omega_s \omega_i)^{1/2} E_p \cdot \frac{2\sqrt{A_s A_i} A_p}{A_p^2 A_i^2 + A_p^2 A_s^2 + A_s^2 A_i^2} \tag{6.65}$$

6.10 Paired Count Rate and Spectral Power Density

We assume that the total loss of the signal and idler fields are the same. The paired count rate is then equal to the photon count rate of the signal (or idler) field and given by

$$\begin{aligned} R_{\text{cav}} &= \left\langle \hat{b}_s^{\text{out}\dagger}(t) \hat{b}_s^{\text{out}}(t) \right\rangle \\ &= \int_{-\infty}^{\infty} \int_{-\infty}^{\infty} d\omega_1 d\omega_2 e^{i\omega_1 t} e^{-i\omega_2 t} \left\langle \hat{b}_s^{\text{out}\dagger}(\omega_1) \hat{b}_s^{\text{out}}(\omega_2) \right\rangle \end{aligned} \quad (6.66)$$

Noting the commutator relation, $[\hat{b}_j^{\text{in}}(\omega_1), \hat{b}_k^{\text{in}\dagger}(\omega_2)] = \frac{1}{2\pi} \delta_{jk} \delta(\omega_1 - \omega_2)$, we have

$$\begin{aligned} &\left\langle \hat{b}_s^{\text{out}\dagger}(\omega_1) \hat{b}_s^{\text{out}}(\omega_2) \right\rangle \\ &= \left\langle [A^*(\omega_1) \hat{b}_s^{\text{in}\dagger}(\omega_1) + B^*(\omega_1) \hat{b}_i^{\text{in}}(\omega_1)] [A(\omega_2) \hat{b}_s^{\text{in}}(\omega_2) + B(\omega_2) \hat{b}_i^{\text{in}\dagger}(\omega_2)] \right\rangle \\ &= B^*(\omega_1) B(\omega_2) \left\langle \hat{b}_i^{\text{in}}(\omega_1) \hat{b}_i^{\text{in}\dagger}(\omega_2) \right\rangle \\ &= B^*(\omega_1) B(\omega_2) \frac{1}{2\pi} \delta(\omega_1 - \omega_2) \end{aligned} \quad (6.67)$$

The paired count rate is then

$$R_{\text{cav}} = \int_{-\infty}^{\infty} S_{\text{cav}}(\omega) d\omega \quad (6.68)$$

where the spectral power density (spectrum) of the signal is given by

$$\begin{aligned} S_{\text{cav}}(\omega) &= \frac{1}{2\pi} |B(\omega)|^2 \\ &= \frac{1}{2\pi} \frac{\gamma_s \gamma_i \kappa_0^2 \text{sinc}^2(\Delta k L / 2)}{\frac{1}{16} [4(\omega - \Omega_q)^2 + \Gamma_s^2] [4(\omega_i - \Omega_r)^2 + \Gamma_i^2] - \frac{1}{2} \kappa^2 [4(\omega - \Omega_q)(\omega_i - \Omega_r) + \Gamma_s \Gamma_i] + \kappa^4} \end{aligned} \quad (6.69)$$

In the *low gain* regime, we drop the κ^2 and κ^4 terms in denominator. The spectrum becomes

$$S_{\text{cav}}(\omega) = \frac{1}{2\pi} \frac{16\gamma_s\gamma_i \kappa_0^2 \text{sinc}^2(\Delta kL/2)}{[4(\omega - \Omega_q)^2 + \Gamma_s^2][4(\omega_i - \Omega_r)^2 + \Gamma_i^2]} \quad (6.70)$$

and the paired count rate is

$$R_{\text{cav}} = \frac{4\gamma_s\gamma_i(\frac{1}{\Gamma_s} + \frac{1}{\Gamma_i})\kappa_0^2 \text{sinc}^2(\Delta kL/2)}{(\Gamma_s + \Gamma_i)^2 + 4(\omega_p - \Omega_q - \Omega_r)^2} \quad (6.71)$$

For $\Gamma_s \approx \Gamma_i \equiv \bar{\Gamma}$ and $\gamma_s \approx \gamma_i \equiv \bar{\gamma}$, the spectrum can be written as

$$\begin{aligned} S_{\text{cav}}(\omega) &= \frac{1}{2\pi} \frac{16 \bar{\gamma}^2 \kappa_0^2 \text{sinc}^2(\Delta kL/2)}{[4(\omega - \Omega_q)^2 + \bar{\Gamma}^2][4(\omega_i - \Omega_r)^2 + \bar{\Gamma}^2]} \\ &= \frac{1}{2\pi} \frac{16 \bar{\gamma}^2 \kappa_0^2 \text{sinc}^2(\Delta kL/2)}{\{4[(\omega - \omega_{s0}) + (\omega_p - \Omega_q - \Omega_r)/2]^2 + \bar{\Gamma}^2\} \{4[(\omega - \omega_{s0}) - (\omega_p - \Omega_q - \Omega_r)/2]^2 + \bar{\Gamma}^2\}} \end{aligned} \quad (6.72)$$

with the central frequency being $\omega_{s0} = (\omega_p + \Omega_q - \Omega_r)/2$ for the signal field and $\omega_{i0} = \omega_p - \omega_{s0} = (\omega_p + \Omega_r - \Omega_q)/2$ for the idler field. The FWHM bandwidth depends on the detuning $(\omega_p - \Omega_q - \Omega_r)/2$

$$\Delta\omega_{\text{cav}} = \sqrt{-\bar{\Gamma}^2 + (\omega_p - \Omega_q - \Omega_r)^2 + \sqrt{2}\sqrt{\bar{\Gamma}^4 + (\omega_p - \Omega_q - \Omega_r)^4}} \quad (6.73)$$

At *exact phase matching*, $\Delta k = 0$, and *zero detuning*, $\delta = (\omega_p - \Omega_q - \Omega_r)/2 = 0$, the paired photon rate has the maximum value of

$$R_{\text{max}} = \frac{4\kappa_0^2\gamma_s\gamma_i}{(\Gamma_s + \Gamma_i)\Gamma_s\Gamma_i} \quad (6.74)$$

and the FWHM bandwidth is minimum

$$\Delta\omega_{\text{res}} = \sqrt{\frac{\sqrt{\Gamma_s^4 + 6\Gamma_s^2\Gamma_i^2 + \Gamma_i^4} - \Gamma_s^2 - \Gamma_i^2}{2}} \quad (6.75)$$

To find out the mirror reflectivity r that maximizes the paired count rate, we assume that the signal and idler fields have the same mirror reflectivity $r_s = r_i = r$ and crystal loss

$\xi_s = \xi_i = \xi$. Then $\partial R_{\max}/\partial r = 0$ gives $r = 1 - 4\xi$.

When phase matching ($\Delta k = 0$) but not double resonance ($\delta \neq 0$) is satisfied, the paired photon rate can be expressed as

$$R = \frac{R_{\max}}{1 + 16(\delta/\bar{\Gamma})^2} \quad (6.76)$$

where we assume $\Gamma_s \approx \Gamma_i \equiv \bar{\Gamma}$.

6.11 Temporal Second-order Intensity Correlation Function

The temporal second-order intensity correlation function of the signal and idler fields is given by

$$\begin{aligned} G^{(2)}(t_1, t_2) &= \left\langle \hat{b}_i^{\text{out}\dagger}(t_2) \hat{b}_s^{\text{out}\dagger}(t_1) \hat{b}_s^{\text{out}}(t_1) \hat{b}_i^{\text{out}}(t_2) \right\rangle \\ &= \int_{-\infty}^{\infty} \int_{-\infty}^{\infty} \int_{-\infty}^{\infty} \int_{-\infty}^{\infty} d\omega_1 d\omega_2 d\omega_3 d\omega_4 e^{i\omega_1 t_2} e^{i\omega_2 t_1} e^{-i\omega_3 t_1} e^{-i\omega_4 t_2} \\ &\quad \cdot \left\langle \hat{b}_i^{\text{out}\dagger}(\omega_1) \hat{b}_s^{\text{out}\dagger}(\omega_2) \hat{b}_s^{\text{out}}(\omega_3) \hat{b}_i^{\text{out}}(\omega_4) \right\rangle \end{aligned} \quad (6.77)$$

where the expectation value can be carried out by using the commutator $[\hat{b}^{\text{in}}(\omega_i), \hat{b}^{\text{in}}(\omega_j)] = \delta(\omega_i - \omega_j)/2\pi$,

$$\begin{aligned} \left\langle \hat{b}_i^{\text{out}\dagger}(\omega_1) \hat{b}_s^{\text{out}\dagger}(\omega_2) \hat{b}_s^{\text{out}}(\omega_3) \hat{b}_i^{\text{out}}(\omega_4) \right\rangle &= \langle [C(-\omega_1) \hat{b}_s^{\text{in}}(-\omega_1) + D(-\omega_1) \hat{b}_i^{\text{in}\dagger}(\omega_1)] \cdot [A^*(\omega_2) \hat{b}_s^{\text{in}\dagger}(\omega_2) + B^*(\omega_2) \hat{b}_i^{\text{in}}(\omega_2)] \\ &\quad \cdot [A(\omega_3) \hat{b}_s^{\text{in}}(\omega_3) + B(\omega_3) \hat{b}_i^{\text{in}\dagger}(\omega_3)] \cdot [C^*(-\omega_4) \hat{b}_s^{\text{in}\dagger}(-\omega_4) + D^*(-\omega_4) \hat{b}_i^{\text{in}}(-\omega_4)] \rangle \\ &= C(-\omega_1) A^*(\omega_2) A(\omega_3) C^*(-\omega_4) \langle \hat{b}_s^{\text{in}}(-\omega_1) \hat{b}_s^{\text{in}\dagger}(\omega_2) \hat{b}_s^{\text{in}}(\omega_3) \hat{b}_s^{\text{in}\dagger}(-\omega_4) \rangle \\ &\quad + C(-\omega_1) B^*(\omega_2) B(\omega_3) C^*(-\omega_4) \langle \hat{b}_s^{\text{in}}(-\omega_1) \hat{b}_i^{\text{in}}(\omega_2) \hat{b}_i^{\text{in}\dagger}(\omega_3) \hat{b}_s^{\text{in}\dagger}(-\omega_4) \rangle \\ &= C(-\omega_1) A^*(\omega_2) A(\omega_3) C^*(-\omega_4) \left(\frac{1}{2\pi}\right)^2 \delta(\omega_1 + \omega_2) \delta(\omega_3 + \omega_4) \\ &\quad + C(-\omega_1) B^*(\omega_2) B(\omega_3) C^*(-\omega_4) \left(\frac{1}{2\pi}\right)^2 \delta(\omega_1 - \omega_4) \delta(\omega_2 - \omega_3) \end{aligned}$$

We then have

$$\begin{aligned}
G^{(2)}(\tau) &= \left| \frac{1}{2\pi} \int_{-\infty}^{\infty} A(\omega) C^{*}(\omega) e^{i\omega\tau} d\omega \right|^2 + \left(\frac{1}{2\pi} \int_{-\infty}^{\infty} |B(\omega)|^2 d\omega \right) \left(\frac{1}{2\pi} \int_{-\infty}^{\infty} |C(\omega)|^2 d\omega \right) \\
&= |\phi(\tau)|^2 + R_{\text{cav}}^2
\end{aligned} \tag{6.79}$$

where $\tau = t_2 - t_1$, R_{cav}^2 is the constant background level resulting from the uncorrelated photons in different pairs, and the biphoton wavefunction $\phi(\tau)$ in the low-gain regime (κ^2 and higher-order terms are dropped) and a lossless cavity is given by

$$\begin{aligned}
\phi(\tau) &= \frac{1}{2\pi} \int_{-\infty}^{\infty} A(\omega) C^{*}(\omega) e^{i\omega\tau} d\omega \\
&\approx \frac{1}{2\pi} \int_{-\infty}^{\infty} \frac{-i\sqrt{\Gamma_s \Gamma_i} \kappa}{(\omega - \Omega_q + i\frac{\Gamma_s}{2})(\omega - \omega_p + \Omega_r - i\frac{\Gamma_i}{2})} e^{i\omega\tau} d\omega \\
&= \frac{2\sqrt{\Gamma_s \Gamma_i} \kappa}{2(\omega_p - \Omega_q - \Omega_r) + i(\Gamma_s + \Gamma_i)} \begin{cases} e^{i\Omega_q\tau + \Gamma_s\tau/2} & , \tau < 0 \\ e^{i(\omega_p - \Omega_r)\tau - \Gamma_i\tau/2} & , \tau > 0 \end{cases}
\end{aligned} \tag{6.80}$$

Substituting $\phi(\tau)$ back to $G^{(2)}(\tau)$, we obtain the biphoton wavepacket in the time domain

$$G^{(2)}(\tau) - R_{\text{cav}}^2 = \frac{4\Gamma_s \Gamma_i \kappa^2}{(\Gamma_s + \Gamma_i)^2 + 4(\omega_p - \Omega_q - \Omega_r)^2} \begin{cases} e^{\Gamma_s\tau} & , \tau < 0 \\ e^{-\Gamma_i\tau} & , \tau > 0 \end{cases} \tag{6.81}$$

6.12 SPDC with Quasi-Phase Matched Backward-wave

The coupled SVEA equations for the backward-wave SPDC with quasi-phase matching are

$$\begin{aligned}
\frac{\partial a_s(\omega, z)}{\partial z} &= i\kappa(z) a_i^\dagger(\omega_i, z) \exp[i\Delta k'(\omega)z] \\
-\frac{\partial a_i^\dagger(\omega_i, z)}{\partial z} &= -i\kappa(z) a_s(\omega, z) \exp[-i\Delta k'(\omega)z]
\end{aligned} \tag{6.82}$$

where $\Delta k'(\omega) = k_p - k_s(\omega) + k_i(\omega_p - \omega)$ and $\kappa(z)$ switches its sign every domain, namely, $\kappa(z) = \kappa_0, -\kappa_0, \kappa_0, \dots$ for the first, second, third, ... domains. The domain length is chosen

to be $l_d = \Lambda_m/2 = m\pi/K_m$ with $K_m = k_p - k_s(\omega_{(Q)}) + k_i(\omega_{i(Q)})$, and $\omega_{(Q)}$ and $\omega_{i(Q)}$ being the m th-order quasi-phase matched signal and idler frequencies, respectively.

In the low gain regime, we can take the driving fields on the right to be independent of z and equal to their values at $z = 0$ for the signal field and $z = L$ for the idler field,

$$\begin{aligned}\frac{\partial a_s(\omega, z)}{\partial z} &= i\kappa(z)a_i^\dagger(\omega_i, L) \exp[i\Delta k'(\omega)z] \\ -\frac{\partial a_i^\dagger(\omega_i, z)}{\partial z} &= -i\kappa(z)a_s(\omega, 0) \exp[-i\Delta k'(\omega)z]\end{aligned}\quad (6.83)$$

Since $\kappa(z)$ is periodic in z with period Λ_m , we can expand $\kappa(z)$ as the summation of its Fourier components,

$$\kappa(z) = \sum_{m=-\infty}^{\infty} c_m \exp(-i2\pi mz/\Lambda_m) \quad (6.84)$$

where

$$\begin{aligned}c_m &= \frac{1}{\Lambda_m} \int_0^{\Lambda_m} \kappa(z) \exp(i2\pi mz/\Lambda_m) dz \\ &= \frac{1}{\Lambda_m} \left[\int_0^{\Lambda_m/2} \kappa_0 \exp(i2\pi mz/\Lambda_m) dz - \int_{\Lambda_m/2}^{\Lambda_m} \kappa_0 \exp(i2\pi mz/\Lambda_m) dz \right] \\ &= \frac{\kappa_0}{im\pi} [\exp(im\pi) - 1] \\ &= \begin{cases} i2\kappa_0/m\pi & \text{if } m \text{ is odd} \\ 0 & \text{if } m \text{ is even} \end{cases}\end{aligned}\quad (6.85)$$

By substituting the Fourier expansion of $\kappa(z)$ back into the coupled equation, we have

$$\frac{\partial a_s(\omega, z)}{\partial z} = -\frac{2\kappa_0}{\pi} \sum_{(m)=-\infty}^{\infty} \frac{1}{m} \exp\{i[\Delta k'(\omega) - K_m]z\} a_i^\dagger(\omega_i, L) \quad (6.86)$$

for the first coupled SVEA equation, where (m) denotes that the summation is only over odd m . Direct integration from $z = 0$ to L then gives

$$a_s(\omega, z) = a_s(\omega, 0) - \frac{2\kappa_0}{\pi} \sum_{(m)=-\infty}^{\infty} \frac{\exp\{i[\Delta k'(\omega) - K_m]L\} - 1}{mi[\Delta k'(\omega) - K_m]} a_i^\dagger(\omega_i, L) \quad (6.87)$$

If K_m is close to $\Delta k'(\omega)$, the summation is dominated by the m th term. We then have

$$a_s(\omega, z) = a_s(\omega, 0) - \frac{2\kappa_0}{m\pi} L \exp\left[\frac{i\Delta k(\omega)L}{2}\right] \text{sinc}\left[\frac{\Delta k(\omega)L}{2}\right] a_i^\dagger(\omega_i, L) \quad (6.88)$$

where $\Delta k(\omega) = k_p - k_s(\omega) + k_i(\omega_p - \omega) - K_m$. Similarly, the second coupled SVEA equation becomes

$$a_i^\dagger(\omega, 0) = a_i^\dagger(\omega, L) - \frac{2\kappa_0}{m\pi} L \exp\left[\frac{-i\Delta k(\omega)L}{2}\right] \text{sinc}\left[\frac{\Delta k(\omega)L}{2}\right] a_s(\omega_i, 0) \quad (6.89)$$

By converting the signal and idler field operators at $z = 0$ and L to the rapidly-varying analytic signals with

$$\begin{aligned} a_s(\omega, z) &= \hat{a}_s(\omega, z) \exp[ik_s(\omega)z] \\ a_i(\omega_i, z) &= \hat{a}_i(\omega_i, z) \exp[ik_i(\omega_i)z] \end{aligned} \quad (6.90)$$

we have

$$\begin{aligned} \hat{a}_s(\omega, L) &= A_1(\omega)\hat{a}_s(\omega, 0) + B_1(\omega)\hat{a}_i^\dagger(\omega_i, L) \\ \hat{a}_i^\dagger(\omega_i, 0) &= C_1(\omega)\hat{a}_s(\omega, 0) + D_1(\omega)\hat{a}_i^\dagger(\omega_i, L) \end{aligned} \quad (6.91)$$

where

$$\begin{aligned}
A_1(\omega) &= \exp[-ik_s(\omega)L] \\
B_1(\omega) &= -\frac{2\kappa_0}{m\pi}L \exp\left[\frac{i\Delta k(\omega)L}{2}\right] \operatorname{sinc}\left[\frac{\Delta k(\omega)L}{2}\right] \exp\{-i[k_s(\omega) + k_i(\omega_i)]L\} \\
C_1(\omega) &= -\frac{2\kappa_0}{m\pi}L \exp\left[\frac{-i\Delta k(\omega)L}{2}\right] \operatorname{sinc}\left[\frac{\Delta k(\omega)L}{2}\right] \\
D_1(\omega) &= \exp[-ik_i(\omega_i)L]
\end{aligned} \tag{6.92}$$

The spectrum of the paired photons is then given by

$$\begin{aligned}
S_1(\omega) &= \frac{1}{2\pi}|B_1(\omega)|^2 \\
&= \frac{\left(\frac{2\kappa_0}{m\pi}\right)^2 L^2}{2\pi} \operatorname{sinc}^2\left[\frac{\Delta k(\omega)L}{2}\right]
\end{aligned} \tag{6.93}$$

where the phase mismatch can be approximated by

$$\begin{aligned}
\Delta k(\omega) &= k_p - k_s(\omega) + k_i(\omega_p - \omega) - K_m \\
&\approx k_p - k_s(\omega_{(Q)}) + k_i(\omega_p - \omega_{(Q)}) - K_m - \frac{n_s^{(g)} + n_i^{(g)}}{c}(\omega - \omega_{(Q)}) \\
&= \frac{n_s^{(g)} + n_i^{(g)}}{c}(\omega_{(Q)} - \omega)
\end{aligned} \tag{6.94}$$

with $n_s^{(g)}$ and $n_i^{(g)}$ being the group indices of the signal and idler fields at $\omega_{(Q)}$ and $\omega_{i(Q)} = \omega_p - \omega_{(Q)}$, respectively. The spectrum can then be written as

$$S_1(\omega) = \frac{\left(\frac{2\kappa_0}{m\pi}\right)^2 L^2}{2\pi} \operatorname{sinc}^2\left[\frac{L(n_s^{(g)} + n_i^{(g)})}{2c}(\omega - \omega_{(Q)})\right] \tag{6.95}$$

with a FWHM bandwidth of

$$\Delta\omega_1 = \frac{1.77 \pi c}{(n_i^{(g)} + n_s^{(g)})L} \tag{6.96}$$

and the paired count rate

$$\begin{aligned}
R_1 &= \int_{-\infty}^{\infty} S_1(\omega) d\omega \\
&= \frac{c \left(\frac{2\kappa_0}{m\pi} \right)^2 L}{n_s^{(g)} + n_i^{(g)}}
\end{aligned} \tag{6.97}$$

6.13 Practical Considerations

Six different system designs are considered. The parameters are calculated based on the following equations and their values are given in Table 1 and Table 2.

6.14 Single Longitudinal-mode

To obtain single longitudinal-mode, we can only allow one pair of signal and idler modes to line up within the gain linewidth. In other words, the spacing between two line-up mode pairs or the *cluster spacing* has to be smaller than the gain linewidth. The cluster spacing can be estimated by

$$\Delta\omega_{cl} = \frac{\Delta_s \Delta_i}{|\Delta_s - \Delta_i|} \tag{6.98}$$

6.15 Tuning Rate

The signal and idler field's cavity resonance frequencies Ω_s and Ω_i can be tuned by changing the temperature T . The thermal expansion coefficient of KTP is about $\alpha = (dL/dT)/L = 10^{-5} \text{ K}^{-1}$. The tuning rate can be estimated as follows.

$$\begin{aligned}
\frac{d\Omega_s}{dT} &\approx -\Omega_s \left(\alpha + n_s^{-1} \frac{dn_s^{(g)}}{dT} \right) \\
\frac{d\Omega_i}{dT} &\approx -\Omega_i \left(\alpha + n_i^{-1} \frac{dn_i^{(g)}}{dT} \right)
\end{aligned} \tag{6.99}$$

where $n_s^{(g)}$ and $n_i^{(g)}$ are the group indices of the signal and idler fields.

6.16 Mode Hopping

As we tune the signal and idler's cavity resonance frequencies by a total amount equal to the difference of their free spectral ranges, mode-hopping will occur. The temperature change corresponding to a mode-hop is

$$\Delta T_{\text{hop}} \approx \frac{\Delta_s - \Delta_i}{\frac{d\Omega_s}{dT} + \frac{d\Omega_i}{dT}} \quad (6.100)$$

where Δ_s and Δ_i are the free spectral ranges of the signal and idler fields, respectively.

6.17 Stabilization

To maintain double resonance for a mode pair, the total amount of change of signal and idler's cavity resonance frequencies has to be smaller than the sum of signal and idler fields' HWHM cavity linewidths. As a result, the temperature has to be stabilized to

$$\Delta T_{\text{stab}} \approx \frac{\frac{\Delta_s}{2F} + \frac{\Delta_i}{2F}}{\frac{d\Omega_s}{dT} + \frac{d\Omega_i}{dT}} \quad (6.101)$$

where F is the cavity finesse.

6.18 Coherence Length and Bandwidth

The coherence length of the biphoton in the time domain will be equal to

$$T_{\text{coh}} = \frac{1}{\Gamma_s} + \frac{1}{\Gamma_i} \quad (6.102)$$

where Γ_s and Γ_i are the power decay rates at the signal and idler frequencies, respectively.

If both phase matching and double resonance are satisfied, the biphoton bandwidth could be as narrow as

$$\Delta\omega_{\text{min}} = \sqrt{\frac{\Gamma_s^4 + 6\Gamma_s^2\Gamma_i^2 + \Gamma_i^4 - \Gamma_s^2 - \Gamma_i^2}{2}} \quad (6.103)$$

6.19 Paired Count Rate and Spectral Brightness

If both phase matching and double resonance are satisfied, for a pump with power $P_{\text{pump}} = 0.01P_{\text{threshold}}$ and beam waist w_0 , the paired count rate could be as high as

$$R_{\text{max}} = \alpha \left(\frac{2}{m\pi}\right)^2 d_{24}^2 \epsilon_0^4 c^4 \eta_s^2 \eta_i^2 \omega_s \omega_i 2\eta_p \frac{P_{\text{pump}}}{\pi(w_0/\sqrt{2})^2} g^2 \frac{\gamma_s \gamma_i}{(\Gamma_s + \Gamma_i) \Gamma_s \Gamma_i} \quad (6.104)$$

where m is the the order of quasi-phase matching and $g \approx 0.5$. We assume confocal condition and take into account the overall detection efficiency α .

The spectral brightness (paired count rate per MHz bandwidth) will be $R_{\text{max}}/\Delta\omega_{\text{min}}$ and the spectral brightness normalized to mW pump power is then $R_{\text{max}}/\Delta\omega_{\text{min}}P_{\text{pump}}$.

To the best of my knowledge, the highest spectral brightness (normalized to mW pump power) reported so far for type-II phase-matched biphotons is from Benson group in 2009, which is

$$\frac{R_{\text{max}}}{\Delta\omega_{\text{min}}P_{\text{pump}}} = 330 \text{ counts}/(\text{s} \cdot \text{MHz} \cdot \text{mW}) \quad (894.3 \text{ nm photons}) \quad (6.105)$$

6.20 Without Cavity

For SPDC without cavity enhancement, the photon rate at pump power P_{pump} is

$$R_{\text{bwd}} = \alpha \frac{\left(\frac{2}{m\pi}\right)^2 d_{24}^2 \epsilon_0^2 c \eta_s \eta_i \omega_s \omega_i 2\eta_p \frac{P_{\text{pump}}}{\pi(w_0/\sqrt{2})^2} L^2 g^2}{|n_s \pm n_i|} \quad (6.106)$$

where the “+” and “-” signs in the denominator correspond to backward-wave and forward-wave, respectively.

	Backward Wave ¹	Cavity-enhanced ²		Forward Wave ³	F =
		F = 1000	F = 1600		
Pump Power = Threshold Power/100	8 W ⁵	766 μ W	445 μ W	8 W ⁵	85
FWHM Bandwidth Δf_{FWHM}	0.081 cm ⁻¹	2.09 MHz	1.44 MHz	1.55 cm ⁻¹	2.09
Biphoton Length	\sim 412 ps	98 ns	143 ns	\sim 21 ps	98
Gain Linewidth	0.081 cm ⁻¹	0.081 cm ⁻¹	0.081 cm ⁻¹	1.55 cm ⁻¹	1.55
Cluster Spacing		1.75 cm ⁻¹	1.75 cm ⁻¹		1.75
Max. Generation Rate (s ⁻¹)	7.10x10 ⁶	1.31x10 ⁵	9.24x10 ⁴	5.42x10 ⁹	3.23x10
Max. Detected Rate R_{max} (s ⁻¹) ⁶	2.09x10 ⁴	385	272	1.59x10 ⁷	
$R_{\text{max}}/\Delta f_{\text{FWHM}}$ (s ⁻¹ MHz ⁻¹)	8.6	184	189	342	
$R_{\text{max}}/\Delta f_{\text{FWHM}}P_{\text{pump}}$ (s ⁻¹ MHz ⁻¹ mW ⁻¹)	0.0011	240	424	0.043	5328
Signal Free Spectral Range		0.094 cm ⁻¹	0.094 cm ⁻¹		0.094
Idler Free Spectral Range		0.089 cm ⁻¹	0.089 cm ⁻¹		0.089
Signal Resonance Frequency Tuning Rate		0.15 cm ⁻¹ /K	0.15 cm ⁻¹ /K		0.15
Idler Resonance Frequency Tuning Rate		0.20 cm ⁻¹ /K	0.20 cm ⁻¹ /K		0.20
Mode-hop Temperature Change		13.7 mK	13.7 mK		13.7
Stability Requirement		0.3 mK	0.2 mK		0.3

Table 1: 3-cm crystals.

	Backward Wave ¹	Cavity-enhanced ²		Forward Wave ³	Ca
		F = 1000	F = 1600		F =
Pump Power = Threshold Power/100	8 W ⁵	1 mW	441 μ W	8 W ⁵	117
FWHM Bandwidth Δf_{FWHM}	0.24 cm ⁻¹	5.61 MHz	3.64 MHz	4.66 cm ⁻¹	5.61
Biphoton Length	\sim 137 ps	37 ns	56 ns	\sim 7 ps	37
Gain Linewidth	0.24 cm ⁻¹	0.24 cm ⁻¹	0.24 cm ⁻¹	4.66 cm ⁻¹	4.66
Cluster Spacing		5.26 cm ⁻¹	5.26 cm ⁻¹		5.26
Max. Generation Rate (s ⁻¹)	7.10x10 ⁶	2.52x10 ⁵	1.52x10 ⁵	5.42x10 ⁹	6.22x10
Max. Detected Rate R_{max} (s ⁻¹) ⁶	2.09x10 ⁴	741	448	1.59x10 ⁷	1828
$R_{\text{max}}/\Delta f_{\text{FWHM}}$ (s ⁻¹ MHz ⁻¹)	2.9	132	123	114	326
$R_{\text{max}}/\Delta f_{\text{FWHM}}P_{\text{pump}}$ (s ⁻¹ MHz ⁻¹ mW ⁻¹)	0.00036	126	279	0.014	2795
Signal Free Spectral Range		0.28 cm ⁻¹	0.28 cm ⁻¹		0.28
Idler Free Spectral Range		0.27 cm ⁻¹	0.27 cm ⁻¹		0.27
Signal Resonance Frequency Tuning Rate		0.15 cm ⁻¹ /K	0.15 cm ⁻¹ /K		0.15 cm
Idler Resonance Frequency Tuning Rate		0.20 cm ⁻¹ /K	0.20 cm ⁻¹ /K		0.20 cm
Mode-hop Temperature Change		41.1 mK	41.1 mK		41.1
Stability Requirement		0.8 mK	0.5 mK		0.8

Table 2: 1-cm crystals.